Advanced GDQ models and 3D stress recovery in multilayered plates, spherical and double-curved panels subjected to transverse shear loads

ADVANCED GDQ MODELS AND 3D STRESS RECOVERY IN MULTILAYERED PLATES, SPHERICAL AND DOUBLE-CURVED PANELS SUBJECTED TO TRANSVERSE SHEAR LOADS

Salvatore Brischetto[1], Francesco Tornabene[2]

ABSTRACT. The present work shows a systematic comparison between different shell models in the case of static analysis of multilayered composite and sandwich plates and spherical shells. Transverse shear loads are applied on these structures. The behavior through the thickness direction is analyzed in terms of the three displacement components and the six stress components. Such evaluations allow to remark the typical zigzag effect of displacements and the interlaminar continuity conditions in terms of congruence and equilibrium equations in the multilayered plates and shells. The boundary load conditions at the external surfaces are also verified. The proposed 3D models are closed form solutions of 3D shell theories developed in the framework of analytical and semi-analytical approaches for differential equations in z. The 2D numerical shell models are classical and refined models developed in both equivalent single layer and layer wise viewpoints. 2D numerical theories are solved by means of the Generalized Differential Quadrature Model (GDQM), which allows general solutions for different boundary conditions, load applications, lamination schemes and geometries. The advantages of this methodology are also clearly shown and discussed for complicated geometries such as double-curved shells.

KEYWORDS: 3D shell theories; 2D advanced shell models; exact solutions; generalized differential quadrature method; exponential matrix solution; sandwich and composite structures; 3D stress recovery; zigzag form; interlaminar continuity.

[1]*DIMEAS – Department of Mechanical and Aerospace Engineering, Politecnico di Torino, Italy.* *salvatore.brischetto@polito.it.*
[2]*DICAM Department - School of Engineering and Architecture, University of Bologna, Italy.* *francesco.tornabene@unibo.it.*

1. INTRODUCTION

Nowadays, in order to obtain higher levels of perfomance, such as the increment of the safety requirements and the improvement of the dynamic behavior, laminated sandwich and composite structures are designed and employed by taking also into account the ratio between the limited weight of the structure and its stiffeness. These kinds of structure are widely used in marine, aerospace, automotive and building engineering fields, where they are modelled as plate and shell elements [1-3]. There existes two different ways to model shell and plate structures, they are the three-dimensional (3D) and the two-dimensional (2D) approaches, in both analytical and numerical forms. The 3D models are characterized by accurate results, but they present a high computational cost due to the large number of degrees of freedom employed to obtain satisfactory solutions. Due to this problem, the 2D shell models are widely used in engineering applications. They present lower computational costs. In fact, a drastic reduction of the computational time and of the complexity of the formulation can be achived by introducing several approximations through the thickness of the structure.

In order to reduce the degrees of freedom of the structural model and to have a simpler formulation, the 2D plate and shell theories were developed in the literature. In fact, the main reason is the reduction of the computational costs. If 2D numerical models are employed, they can consider more complicated problems for the loads, the boundary conditions and the lamination schemes. The Finite Element Method (FEM) is the most popular numerical method available in the literature and it is based on the weak form of the problem. In the latest years, various approches based on the strong form of the problem were proposed. One of them was the Generalized Differential Quadrature (GDQ) method improved by Shu (see [4, 5]). This methodology was applied to several examples in the literature for the analysis of composite and sandwich structures as reported in the works [6-15]. In particular, classical and refined 2D models for the analysis of plates and doubly-curved shells, using the differential geometry, were developed by Tornabene and his co-authors [6-15]. In the paper [16], the free vibration analysis of doubly-curved laminated shells and plates was considered using general higher-order shear deformation theories. The same 2D higher models was used to study the static analysis of doubly-curved laminated shells and panels in [17]. In the work [18], an extension of the Carrera Unified Formulation [19, 20] was proposed to solve completely doubly-curved shell structures. In [21], the static behaviour of doubly-curved anisotropic shells and panels was analysed using the same formulation employed in [18]. Furthermore, Tornabene and his co-authros [21-24] proposed “a posteriori” shear and normal stress in order to obtain the correct stress and strain behaviour through the thickness of the structure.

The analytical 3D formulations presented in the literature have a restricted range of applications due to the limitations derived from the theoretical approach. For these reasons, the numerical 3D approches could be used to avoid these limitations. Among analytical 3D formulations, Pagano [25-27] studied several benchmarks for laminated composite and sandwich plates, these benchmarks are frequently used in the literature for comparisons with other analytical and numerical models. Xu and Zhou [28] proposed a 3D numerical plate model for analyzing the bending behaviour of variable thickness plates. Meyer-Piening [29] studied layered structures with soft cores. A 3D mixed analytical plate solution was proposed by Demasi [30]. Furthermore, Ren [31] analysed the 3D bending solution of composite cylindrical panels under transverse normal loads. An exact 3D solution for composite cylinders subjected to transverse normal loads was proposed by Varadan and Bhaskar [32]. Fan and Zhang [33, 34] analyzed composite spherical panels. A similar formulation for composite cylinders subjected to harmonic loads was proposed by Soldatos and Ye [35]. Another three-dimensional solution for composite plates was proposed by Fan and Ye [36] considering classical load applications. Kashtalyan [37] extended the typical 3D plate solution to the static analysis of single-layered Functionally Graded Material (FGM) structures. Kashtalyan and Menshykova [38] considered sandwich plates embedding FGM cores. Further 3D free vibration and dynamic studies for plates were proposed in the works [39-42]. Similar behaviours were considered for shell structures in the works [43-45]. Furthermore, 3D numerical solutions for free vibration, dynamic and bending analysis of plate and shell structures can be found in the works [46-51]. Recently, Brischetto obtained an analytical 3D exact solution for plates, cylinders and spherical/cylindrical shell panels considering isotropic, composite and functionally graded layers. In the works [52-55], the free vibration analyses of one-layered, laminated composite, sandwich, functionally graded and single-walled carbon nanotube structures was considered. The static analyses for multilayered composite, sandwich and functionally graded plates and shells were proposed in works [56-59]. Brischetto [52-59] used a 3D exact model based on the exponenetial matrix method. The layer-wise approach, the interlaminar continuity conditions in terms of displacements and transverse stresses and the 3D equilibrium equations in mixed orthogonal curvilinear coordinates are the main features of this model. This approach is a sort of generalization of some less general models already presented in the literure [34, 35, 41].

In the presert new paper, analytical and semi-analytical three-dimensional (3D) shell models are used to compare the 2D GDQ solutions obtained with the same recovery procedure adopted in [21-24]. The static analysis of laminated composite/sandwich plates and spherical or double-curved shells, subjected to transverse shear loads

applied at the top surface, is shown in the present paper in analogy with the cases already analyzed in [60] where a transverse normal load is applied at the top, and a different geometry for double-curved shells was considered. Two different closed-form three-dimensional shell theories are here used to compare the accuracy of classical and refined GDQ shell models by Tornabene [5-10], [16-18], [21, 22]. The proposed refined and classical 2D GDQ theories consider the "a posteriori" shear and normal stress recovery in order to correctly evaluate the quantitities through the thickness direction. The 3D formulation based on the Exponential Matrix method, and here called as 3D EM, was developed by Brischetto in [52-59] using mixed orthogonal curvilinear coordinates, interlaminar continuity for transverse stresses and displacements, layer-wise approach and exponential matrix methodology for the analytical resolution of differential equations in the normal direction. The new 3D formulation, presented for the first time in [60] and called 3D GDQ, is based on mixed orthogonal curvilinear coordinates, interlaminar continuity for transverse stresses and displacements, layer-wise approach and the GDQ method by Tornabene [5-10], [16-18], [21-22] to numerically solve the differential equations in the normal direction.

2. 3D GENERAL SHELL THEORIES

The first proposed 3D shell theory uses the 3D equilibrium equations written in mixed curvilinear orthogonal coordinates (s_1, s_2, ζ) [60]. These mixed curvilinear coordinates are indicated in Figure 1 where the meaning of geometry, thickness coordinates, mean radii of curvature $R_1(s_1, s_2)$ and $R_2(s_1, s_2)$ along the two directions s_1 and s_2 are clearly shown. For a general lamina k, the 3D stress state in the material reference system can be given as:

$$\begin{bmatrix} \sigma_1^{(k)} \\ \sigma_2^{(k)} \\ \tau_{12}^{(k)} \\ \tau_{13}^{(k)} \\ \tau_{23}^{(k)} \\ \sigma_3^{(k)} \end{bmatrix} = \begin{bmatrix} \bar{C}_{11}^{(k)} & \bar{C}_{12}^{(k)} & \bar{C}_{16}^{(k)} & 0 & 0 & \bar{C}_{13}^{(k)} \\ \bar{C}_{12}^{(k)} & \bar{C}_{22}^{(k)} & \bar{C}_{26}^{(k)} & 0 & 0 & \bar{C}_{23}^{(k)} \\ \bar{C}_{16}^{(k)} & \bar{C}_{26}^{(k)} & \bar{C}_{66}^{(k)} & 0 & 0 & \bar{C}_{36}^{(k)} \\ 0 & 0 & 0 & \bar{C}_{44}^{(k)} & \bar{C}_{45}^{(k)} & 0 \\ 0 & 0 & 0 & \bar{C}_{45}^{(k)} & \bar{C}_{55}^{(k)} & 0 \\ \bar{C}_{13}^{(k)} & \bar{C}_{23}^{(k)} & \bar{C}_{36}^{(k)} & 0 & 0 & \bar{C}_{33}^{(k)} \end{bmatrix} \begin{bmatrix} \varepsilon_1^{(k)} \\ \varepsilon_2^{(k)} \\ \gamma_{12}^{(k)} \\ \gamma_{13}^{(k)} \\ \gamma_{23}^{(k)} \\ \varepsilon_3^{(k)} \end{bmatrix} \tag{1}$$

The geometrical relations for a spherical shell degenerate into those for cylindrical panels, cylinders and plates by means of simple considerations about the radii of curvature:

$$\begin{bmatrix} \varepsilon_1^{(k)} \\ \varepsilon_2^{(k)} \\ \gamma_{12}^{(k)} \\ \gamma_{13}^{(k)} \\ \gamma_{23}^{(k)} \\ \varepsilon_3^{(k)} \end{bmatrix} = \begin{bmatrix} \frac{1}{H_1^{(k)}}\frac{\partial}{\partial s_1} & 0 & \frac{1}{H_1^{(k)}R_1} \\ 0 & \frac{1}{H_2^{(k)}}\frac{\partial}{\partial s_2} & \frac{1}{H_2^{(k)}R_2} \\ \frac{1}{H_2^{(k)}}\frac{\partial}{\partial s_2} & \frac{1}{H_1^{(k)}}\frac{\partial}{\partial s_1} & 0 \\ \frac{\partial}{\partial \zeta^{(k)}} - \frac{1}{H_1^{(k)}R_1} & 0 & \frac{1}{H_1^{(k)}}\frac{\partial}{\partial s_1} \\ 0 & \frac{\partial}{\partial \zeta^{(k)}} - \frac{1}{H_2^{(k)}R_2} & \frac{1}{H_2^{(k)}}\frac{\partial}{\partial s_2} \\ 0 & 0 & \frac{\partial}{\partial \zeta^{(k)}} \end{bmatrix} \begin{bmatrix} U_1^{(k)} \\ U_2^{(k)} \\ U_3^{(k)} \end{bmatrix} \tag{2}$$

The 3D equilibrium equations in mixed curvilinear orthogonal coordinates for the general case of spherical shell panels are:

$$\begin{aligned} &\frac{1}{H_1^{(k)}}\frac{\partial \sigma_1^{(k)}}{\partial s_1} + \frac{1}{H_2^{(k)}}\frac{\partial \tau_{12}^{(k)}}{\partial s_2} + \frac{\partial \tau_{13}^{(k)}}{\partial \zeta^{(k)}} + \tau_{13}^{(k)}\left(\frac{2}{H_1^{(k)}R_1} + \frac{1}{H_2^{(k)}R_2}\right) + f_1^{(k)} = 0 \\ &\frac{1}{H_2^{(k)}}\frac{\partial \sigma_2^{(k)}}{\partial s_2} + \frac{1}{H_1^{(k)}}\frac{\partial \tau_{12}^{(k)}}{\partial s_1} + \frac{\partial \tau_{23}^{(k)}}{\partial \zeta^{(k)}} + \tau_{23}^{(k)}\left(\frac{1}{H_1^{(k)}R_1} + \frac{2}{H_2^{(k)}R_2}\right) + f_2^{(k)} = 0 \\ &\frac{1}{H_1^{(k)}}\frac{\partial \tau_{13}^{(k)}}{\partial s_1} + \frac{1}{H_2^{(k)}}\frac{\partial \tau_{23}^{(k)}}{\partial s_2} + \frac{\partial \sigma_3^{(k)}}{\partial \zeta^{(k)}} + \sigma_3^{(k)}\left(\frac{1}{H_1^{(k)}R_1} + \frac{1}{H_2^{(k)}R_2}\right) - \frac{\sigma_1^{(k)}}{H_1^{(k)}R_1} - \frac{\sigma_2^{(k)}}{H_2^{(k)}R_2} + f_3^{(k)} = 0 \end{aligned} \tag{3}$$

where the parametric coefficients $H_1^{(k)}$ and $H_2^{(k)}$ are expressed as functions of the thickness coordinate and radii of curvature:

$$\begin{aligned} H_1^{(k)} &= 1 + \frac{\zeta}{R_1} \\ H_2^{(k)} &= 1 + \frac{\zeta}{R_2} \end{aligned} \tag{4}$$

In the equations (1)-(3), $U_1(s_1, s_2, \zeta)$, $U_2(s_1, s_2, \zeta)$ and $U_3(s_1, s_2, \zeta)$ are the displacements. $f_i^{(k)}$ indicates the body forces. $\varepsilon_1^{(k)}, \varepsilon_2^{(k)}, \gamma_{12}^{(k)}, \gamma_{13}^{(k)}, \gamma_{23}^{(k)}, \varepsilon_3^{(k)}$ and $\sigma_1^{(k)}, \sigma_2^{(k)}, \tau_{12}^{(k)}, \tau_{13}^{(k)}, \tau_{23}^{(k)}, \sigma_3^{(k)}$ are the strain and stress components defined in each k lamina, respectively. The closed form solution is obtained only if cross-ply configurations are considered (angles equal 0 or 90). This feature means coefficients $\bar{C}_{16}^{(k)} = \bar{C}_{26}^{(k)} = \bar{C}_{36}^{(k)} = \bar{C}_{45}^{(k)} = 0$ in the consitutive relations explicitly written in Eq. (1) (see Reddy's book [1]). Moreoves, plates and shells must have all the sides as simply supported, which means harmonic forms for displacements, stresses, loads and body forces:

$$\left\{U_1^{(k)},\, f_1^{(k)},\tau_{13}^{(k)}\right\}(s_1,s_2,\zeta)=\left\{\mathrm{U}_1^{(k)},\mathrm{f}_1^{(k)},\mathrm{T}_{13}^{(k)}\right\}(\zeta)\cos\left(\frac{n\pi}{L_1}s_1\right)\sin\left(\frac{m\pi}{L_2}s_2\right) \tag{5}$$

$$\left\{U_2^{(k)},\, f_2^{(k)},\tau_{23}^{(k)}\right\}(s_1,s_2,\zeta)=\left\{\mathrm{U}_2^{(k)},\mathrm{f}_2^{(k)},\mathrm{T}_{23}^{(k)}\right\}(\zeta)\sin\left(\frac{n\pi}{L_1}s_1\right)\cos\left(\frac{m\pi}{L_2}s_2\right) \tag{6}$$

$$\left\{U_3^{(k)},\, f_3^{(k)},\sigma_1^{(k)},\sigma_2^{(k)},\sigma_3^{(k)}\right\}(s_1,s_2,\zeta)=\left\{\mathrm{U}_3^{(k)},\mathrm{f}_3^{(k)},\Sigma_1^{(k)},\Sigma_2^{(k)},\Sigma_3^{(k)}\right\}(\zeta)\sin\left(\frac{n\pi}{L_1}s_1\right)\sin\left(\frac{m\pi}{L_2}s_2\right) \tag{7}$$

$$\tau_{12}^{(k)}(s_1,s_2,\zeta)=\mathrm{T}_{12}^{(k)}(\zeta)\cos\left(\frac{n\pi}{L_1}s_1\right)\cos\left(\frac{m\pi}{L_2}s_2\right) \tag{8}$$

where m and n are the half-wave numbers, and L_1 and L_2 are the dimensions of the structures. $\mathrm{U}_1^{(k)}$, $\mathrm{U}_2^{(k)}$, $\mathrm{U}_3^{(k)}$, $\mathrm{f}_1^{(k)}$, $\mathrm{f}_2^{(k)}$, $\mathrm{f}_3^{(k)}$, $\mathrm{T}_{13}^{(k)}$, $\mathrm{T}_{23}^{(k)}$, $\mathrm{T}_{12}^{(k)}$, $\Sigma_1^{(k)}$, $\Sigma_2^{(k)}$ and $\Sigma_3^{(k)}$ are the relative amplitudes.

The closed form of differential equations is obtained after the inclusion of Eqs.(5)-(8) in Eqs.(3) written in displacement form by means of constitutive and geometrical equations (1) and (2):

$$\begin{aligned}&\left(\bar{C}_{44}^{(k)}\frac{\partial^2}{\partial\zeta^2}+\left(\frac{\bar{C}_{44}^{(k)}}{H_1^{(k)}R_1}+\frac{\bar{C}_{44}^{(k)}}{H_2^{(k)}R_2}\right)\frac{\partial}{\partial\zeta}-\frac{n^2\pi^2}{L_1^2}\frac{\bar{C}_{11}^{(k)}}{H_1^{(k)2}}-\frac{m^2\pi^2}{L_2^2}\frac{\bar{C}_{66}^{(k)}}{H_2^{(k)2}}-\frac{\bar{C}_{44}^{(k)}}{H_1^{(k)}H_2^{(k)}R_1R_2}-\frac{\bar{C}_{44}^{(k)}}{H_1^{(k)2}R_1^2}\right)\mathrm{U}_1^{(k)}+\\&+\left(-\frac{n\pi}{L_1}\frac{m\pi}{L_2}\frac{\bar{C}_{12}^{(k)}+\bar{C}_{66}^{(k)}}{H_1^{(k)}H_2^{(k)}}\right)\mathrm{U}_2^{(k)}+\left(\frac{n\pi}{L_1}\frac{\bar{C}_{13}^{(k)}+\bar{C}_{44}^{(k)}}{H_1^{(k)}}\frac{\partial}{\partial\zeta}+\frac{n\pi}{L_1}\left(\frac{\bar{C}_{12}^{(k)}+\bar{C}_{44}^{(k)}}{H_1^{(k)}H_2^{(k)}R_2}+\frac{\bar{C}_{11}^{(k)}+\bar{C}_{44}^{(k)}}{H_1^{(k)2}R_1}\right)\right)\mathrm{U}_3^{(k)}+\mathrm{f}_1^{(k)}=0\end{aligned} \tag{9}$$

$$\begin{aligned}&\left(-\frac{n\pi}{L_1}\frac{m\pi}{L_2}\frac{\bar{C}_{12}^{(k)}+\bar{C}_{66}^{(k)}}{H_1^{(k)}H_2^{(k)}}\right)\mathrm{U}_1^{(k)}+\left(\bar{C}_{55}^{(k)}\frac{\partial^2}{\partial\zeta^2}+\left(\frac{\bar{C}_{55}^{(k)}}{H_1^{(k)}R_1}+\frac{\bar{C}_{55}^{(k)}}{H_2^{(k)}R_2}\right)\frac{\partial}{\partial\zeta}-\frac{n^2\pi^2}{L_1^2}\frac{\bar{C}_{66}^{(k)}}{H_1^{(k)2}}-\frac{m^2\pi^2}{L_2^2}\frac{\bar{C}_{22}^{(k)}}{H_2^{(k)2}}-\frac{\bar{C}_{55}^{(k)}}{H_1^{(k)}H_2^{(k)}R_1R_2}-\frac{\bar{C}_{55}^{(k)}}{H_2^{(k)2}R_2^2}\right)\mathrm{U}_2^{(k)}+\\&+\left(\frac{m\pi}{L_2}\frac{\bar{C}_{23}^{(k)}+\bar{C}_{55}^{(k)}}{H_2^{(k)}}\frac{\partial}{\partial\zeta}+\frac{m\pi}{L_2}\left(\frac{\bar{C}_{12}^{(k)}+\bar{C}_{55}^{(k)}}{H_1^{(k)}H_2^{(k)}R_1}+\frac{\bar{C}_{22}^{(k)}+\bar{C}_{55}^{(k)}}{H_2^{(k)2}R_2}\right)\right)\mathrm{U}_3^{(k)}+\mathrm{f}_2^{(k)}=0\end{aligned} \tag{10}$$

$$\begin{aligned}&\left(-\frac{n\pi}{L_1}\frac{\bar{C}_{13}^{(k)}+\bar{C}_{44}^{(k)}}{H_1^{(k)}}\frac{\partial}{\partial\zeta}-\frac{n\pi}{L_1}\left(\frac{\bar{C}_{13}^{(k)}-\bar{C}_{12}^{(k)}}{H_1^{(k)}H_2^{(k)}R_2}-\frac{\bar{C}_{11}^{(k)}+\bar{C}_{44}^{(k)}}{H_1^{(k)2}R_1}\right)\right)\mathrm{U}_1^{(k)}+\left(-\frac{m\pi}{L_2}\frac{\bar{C}_{23}^{(k)}+\bar{C}_{55}^{(k)}}{H_2^{(k)}}\frac{\partial}{\partial\zeta}-\frac{m\pi}{L_2}\left(\frac{\bar{C}_{23}^{(k)}-\bar{C}_{12}^{(k)}}{H_1^{(k)}H_2^{(k)}R_1}-\frac{\bar{C}_{22}^{(k)}+\bar{C}_{55}^{(k)}}{H_2^{(k)2}R_2}\right)\right)\mathrm{U}_2^{(k)}+\\&+\left(\bar{C}_{33}^{(k)}\frac{\partial^2}{\partial\zeta^2}+\left(\frac{\bar{C}_{33}^{(k)}}{H_1^{(k)}R_1}+\frac{\bar{C}_{33}^{(k)}}{H_2^{(k)}R_2}\right)\frac{\partial}{\partial\zeta}-\frac{n^2\pi^2}{L_1^2}\frac{\bar{C}_{44}^{(k)}}{H_1^{(k)2}}-\frac{m^2\pi^2}{L_2^2}\frac{\bar{C}_{55}^{(k)}}{H_2^{(k)2}}+\frac{\bar{C}_{13}^{(k)}+\bar{C}_{23}^{(k)}-2\bar{C}_{12}^{(k)}}{H_1^{(k)}H_2^{(k)}R_1R_2}-\frac{\bar{C}_{11}^{(k)}}{H_1^{(k)2}R_1^2}-\frac{\bar{C}_{22}^{(k)}}{H_2^{(k)2}R_2^2}\right)\mathrm{U}_3^{(k)}+\mathrm{f}_3^{(k)}=0\end{aligned} \tag{11}$$

The proposed 3D theory is developed in layer-wise form and it uses the equilibrium conditions for transverse stresses at each interface:

$$\begin{aligned}\tau_{13}^{(k)}(s_1,s_2,\zeta_{k+1})&=\tau_{13}^{(k+1)}(s_1,s_2,\zeta_{k+1})\\\tau_{23}^{(k)}(s_1,s_2,\zeta_{k+1})&=\tau_{23}^{(k+1)}(s_1,s_2,\zeta_{k+1})\\\sigma_{33}^{(k)}(s_1,s_2,\zeta_{k+1})&=\sigma_{33}^{(k+1)}(s_1,s_2,\zeta_{k+1})\end{aligned} \tag{12}$$

and the compatibility conditions for displacements at each interfaces:

$$
\begin{aligned}
U_1^{(k)}\left(s_1,s_2,\zeta_{k+1}\right) &= U_1^{(k+1)}\left(s_1,s_2,\zeta_{k+1}\right)\\
U_2^{(k)}\left(s_1,s_2,\zeta_{k+1}\right) &= U_2^{(k+1)}\left(s_1,s_2,\zeta_{k+1}\right)\\
U_3^{(k)}\left(s_1,s_2,\zeta_{k+1}\right) &= U_3^{(k+1)}\left(s_1,s_2,\zeta_{k+1}\right)
\end{aligned}
\tag{13}
$$

The load conditions at the external surfaces of the proposed benchmarks consider only transverse shear loads in terms of stress $\tau_{23}^{(1,l)}$ in harmonic form:

$$
\tau_{23}^{(1,l)}\left(s_1,s_2,\pm\frac{h}{2}\right) = q_2^{(1,l)}\left(s_1,s_2\right) = \mathrm{q}_2^{(\pm)}\sin\left(\frac{n\pi}{L_1}s_1\right)\cos\left(\frac{m\pi}{L_2}s_2\right) \tag{14}
$$

The closed form of the sistem of partial differential equations in ζ (see Eqs. (9)-(11)) can be solved in pure analytical form using the Exponential Matrix (EM) method (see details in [52-59]):

$$
\mathbf{U}^{(j)}\left(\tilde{z}^j\right) = \exp\left(\mathbf{A}^{j*}\tilde{z}^j\right)\mathbf{U}^{(j)}\left(0\right) \quad \text{with} \quad \tilde{z}^j \in \left[0,h^j\right] \tag{15}
$$

In the present paper this solution is defined as “3D EM”, and it was extensively described in [52-59]. In [52-59], the “3D EM” solution was also validated using different 3D analytical and numerical solutions developed for particular geometries. Some of these comparisons were those with the 3D plate solution by Pagano [25-27], with the 3D solution by Ren [31] for static analysis of laminated cylindrical panels, with the exact 3D solution by Varadan and Bhaskar [32] for the bending of composite cylinders, with the 3D exact solutions by Fan and Zhang [33] developed for thick composite spherical shells, with the exact elastic model by Soldatos and Ye [35] for hollow cylinders, with the 3D exact model by Kashtalyan [37] and Kashtalyan and Menshykova [38] for static analysis of one-layered and sandwich functionally graded plates, with the 3D model by Vel and Batra [39] for the vibration analysis of functionally graded plates and with the 3D exact solution by Messina [41] for the mode investigation of multilayered composite plates.

The second 3D shell model here proposed is defined as “3D GDQ”. The only difference in the solution procedure seen in Eqs. (1)-(15) is the use of the Generalized Differential Quadrature model (GDQ) in place of the Exponential Matrix (EM) method for the solution of partial differential equations in ζ given in closed form. The GDQ method is a powerful numerical procedure extensively and successfully applied by the second author in his past works [5-10], [16-18] and [21-24] where the GDQ method was dedicated to the building of refined 2D numerical shell models. In brief, in the case of a one-dimensional domain using an interval $\left[x_1,x_T\right]$, the GDQ method allows the approximation of the n-th derivative in a generic point x_i of a sufficiently smooth function $f\left(x\right)$ using a weighted linear sum of the function values at a certain number of defined points

$$\left.\frac{d^n f(x)}{dx^n}\right|_{x=x_i} \cong \sum_{j=1}^{T} \varsigma_{ij}^{(n)} f(x_j) \tag{16}$$

where i = 1, 2,..., T , with T indicating the total number of grid points. The weighting coefficients are defined as $\varsigma_{ij}^{(n)}$ and they are calculated by means of the recursive relations given by Shu in [5], and then used in[24]. Eq.(16) is used in place of Eq.(15). This numerical method permits the calculation of the derivative of a function in each point of the proposed domain. The nodes in the domain are given in accordance with a specific grid distribution. In this proposed 3D shell solution, the Chebyshev-Gauss-Lobatto grid distribution is employed due to its stability and accuracy as demonstrated in [5] and [24]. The discrete points are given as

$$x_i = \left(1 - \cos\left(\frac{i-1}{T-1}\pi\right)\right)\frac{\left(x_T - x_1\right)}{2} + x_1 \tag{17}$$

where $i = 1, 2, ..., T$ and $x \in \left[x_1, x_T\right]$. The numerical solution, by means of the GDQ method, of partial differential equations in ζ given in eqs. (9)-(11) allows the reduction of the computational cost. This feature does not modify the precision of the results as will be demonstrated in the section 4 where "3D EM" and "3D GDQ" theories are very close for all the proposed benchmarks. Therefore, the new 3D GDQ model will be considered as validated for the static investigation of multilayered anisotropic plates and spherical shells thanks the comparisons with the 3D EM shell solution already verified in [52-59].

3. EQUIVALENT SINGLE LAYER AND LAYER WISE 2D GDQ SHELL MODELS

The present formulation for doubly-curved surfaces is based on the differential geometry as described in the book [61]. A reference surface is defined and the two-dimensional models for generic doubly-curved shells are strictly related to the mechanical behavior of this reference surface. The reference surface is the middle surface of a multilayered shell as indicated in Figure 1. The 3D shell is positioned in the global reference system $Ox_1x_2x_3$. The thickness of the shell is the distance from the bottom external curved surface and the top external curved surface. The global thickness of a multilayered shell is:

$$h = \sum_{k=1}^{l} h_k \tag{18}$$

where h_k is the thickness of the k layer. A local reference system $O'\alpha_1\alpha_2\zeta$ is also defined as shown Figure 1. The boundary limits of the shell are:

$$\begin{aligned}\alpha_1 &\in \left[\alpha_1^0, \alpha_1^1\right] \\ \alpha_2 &\in \left[\alpha_2^0, \alpha_2^1\right] \\ \zeta &\in \left[-h/2, h/2\right]\end{aligned} \tag{19}$$

The curvilinear orthogonal coordinates α_1, α_2 are the lines of principal curvature of the shell reference surface as demonstrated in the book [61]. In generic cases, $\alpha_1 = \varphi, \alpha_2 = \vartheta$ for shells of revolution, $\alpha_1 = \varphi, \alpha_2 = y$ for single-curved panels of translation, $\alpha_1 = s_1 = x, \alpha_2 = s_2 = y$ for a rectangular plate. Each point P of the three-dimensional shell is defined using the following vector:

$$\mathbf{R}\left(\alpha_1, \alpha_2, \zeta\right) = \mathbf{r}\left(\alpha_1, \alpha_2\right) + \frac{h}{2} z \mathbf{n}\left(\alpha_1, \alpha_2\right) \tag{20}$$

where $z = 2\zeta / h\left(\alpha_1, \alpha_2\right) \in \left[-1, 1\right]$ is a no-dimensional variable. $\mathbf{r}\left(\alpha_1, \alpha_2\right)$ is the position vector indicating each point on the reference surface. $\mathbf{n}\left(\alpha_1, \alpha_2\right)$ is the outward unit normal

$$\mathbf{n} = \frac{\mathbf{r}_{,1} \wedge \mathbf{r}_{,2}}{\left|\mathbf{r}_{,1} \wedge \mathbf{r}_{,2}\right|} \tag{21}$$

where $\mathbf{r}_{,i} = \partial \mathbf{r} / \partial \alpha_i$, for $i = 1, 2$. The symbol "$\wedge$" is used to indicate the vector product. The position vector $\mathbf{r}\left(\alpha_1, \alpha_2\right)$ allows the calculation of the first fundamental forms of the reference surface [61]. The Lamè parameters $A_1\left(\alpha_1, \alpha_2\right)$ and $A_2\left(\alpha_1, \alpha_2\right)$ are defined as

$$\begin{aligned}A_1 &= \sqrt{\mathbf{r}_{,1} \cdot \mathbf{r}_{,1}} \\ A_2 &= \sqrt{\mathbf{r}_{,2} \cdot \mathbf{r}_{,2}}\end{aligned} \tag{22}$$

where the symbol "$\cdot$" indicates the scalar product. The principal radii of curvature of the surface $R_1\left(\alpha_1, \alpha_2\right)$ and $R_2\left(\alpha_1, \alpha_2\right)$ are given as

$$\begin{aligned}R_1 &= -\frac{\mathbf{r}_{,1} \cdot \mathbf{r}_{,1}}{\mathbf{r}_{,11} \cdot \mathbf{n}} \\ R_2 &= -\frac{\mathbf{r}_{,2} \cdot \mathbf{r}_{,2}}{\mathbf{r}_{,22} \cdot \mathbf{n}}\end{aligned} \tag{23}$$

For a generic doubly-curved shell, the principal radii of curvature change in each point of the domain. The presented formulation can be used for static and dynamic investigations of thick and moderately thick shells

$$0.01 \le \max\left(\frac{h}{R_{\min}}, \frac{h}{L_{\min}}\right) \le 0.2 \tag{24}$$

$R_{\min}$ and $L_{\min}$ indicate the minimum radius of curvature and the lowest size of the structure, respectively. The three displacement components $\boldsymbol{U}(\alpha_1,\alpha_2,\zeta)=\{U_1(\alpha_1,\alpha_2,\zeta)U_2(\alpha_1,\alpha_2,\zeta)U_3(\alpha_1,\alpha_2,\zeta)\}^T$ of a generic shell are expressed using the Carrera Unified Formulation [61]. The displacement field can be written as

$$\boldsymbol{U}=F_0\,\boldsymbol{u}^{(0)}+F_1\,\boldsymbol{u}^{(1)}+F_2\,\boldsymbol{u}^{(2)}+F_3\,\boldsymbol{u}^{(3)}+...+F_N\boldsymbol{u}^{(N)}+F_{N+1}\boldsymbol{u}^{(N+1)} \tag{25}$$

Where the generalized displacement vector is $\boldsymbol{u}^{(\tau)}(\alpha_1,\alpha_2)=\{u_1^{(\tau)}(\alpha_1,\alpha_2)u_2^{(\tau)}(\alpha_1,\alpha_2)u_3^{(\tau)}(\alpha_1,\alpha_2)\}^T$. $F_\tau=F_\tau(\zeta)$ are the thickness functions as explicitly given in [61]. Modifying the order of expansion and the type of thickness functions, different kinematic models can be obtained. Eq.(25) does not show the dependence on the k-th layer, therefore it is written for the Equivalent Single Layer (ESL) models. Classical theories such as the Reissner-Mindlin theory or the Kirchhoff theory can be obtained as particular cases. The Murakami's zigzag function $\mathrm{Z}=\mathrm{Z}(\zeta)$ can be added as the $(N+1)$-th degree of freedom in ESL models in order to recover the typical zig-zag effect through the thickness of the structure. The Murakami's zigzag function is defined as

$$\mathrm{Z}=(-1)^k\left(\frac{2}{\zeta_{k+1}-\zeta_k}\zeta-\frac{\zeta_{k+1}+\zeta_k}{\zeta_{k+1}-\zeta_k}\right) \tag{26}$$

where ζ_k is the coordinate of the k-th layer through the thickness direction ζ. Murakami's function has been detailed in [61]. The ESL theories employed in this paper use the power functions ζ^τ as thickness functions, where $\tau=0,1,2,...,N$ [61]. The following theories are obtained for $N\le 4$ using the following acronyms: ED1 for N=1 and EDZ1 for N=1 and the use of $\mathrm{Z}=\mathrm{Z}(\zeta)$, ED2 for N=2 and EDZ2 for N=2 and the use of $\mathrm{Z}=\mathrm{Z}(\zeta)$, ED3 for N=3 and EDZ3 for N=3 and the use of $\mathrm{Z}=\mathrm{Z}(\zeta)$, and ED4 for N=4 and EDZ4 for N=4 and the use of $\mathrm{Z}=\mathrm{Z}(\zeta)$. "E" indicates ESL, "D" indicates that the generalized displacements are the main variables of the problem, "Z" indicates the Murakami's zigzag function. The vector $\boldsymbol{\varepsilon}^{(\tau)}=\boldsymbol{\varepsilon}^{(\tau)}(\alpha_1,\alpha_2)$ of τ-th order generalized strain components on the reference surface is:

$$\boldsymbol{\varepsilon}^{(\tau)}=\left[\varepsilon_1^{(\tau)}\quad\varepsilon_2^{(\tau)}\quad\gamma_1^{(\tau)}\quad\gamma_2^{(\tau)}\quad\gamma_{13}^{(\tau)}\quad\gamma_{23}^{(\tau)}\quad\omega_{13}^{(\tau)}\quad\omega_{23}^{(\tau)}\quad\varepsilon_3^{(\tau)}\right]^T \tag{27}$$

The τ-th order generalized strain component vector is linked to the τ-th order generalized displacement component vector $\mathbf{u}^{(\tau)}$ by means of the following compact form

$$\boldsymbol{\varepsilon}^{(\tau)}=\mathbf{D}_\Omega\mathbf{u}^{(\tau)} \tag{28}$$

the operator $\mathbf{D}_\Omega$ has both differential and geometrical contributions and it has been detailed in [61].

The vector of the stress resultants is $\mathbf{S}^{(\tau)} = \mathbf{S}^{(\tau)}\left(\alpha_1, \alpha_2\right)$ for the τ -th order of kinematic expansion

$$\mathbf{S}^{(\tau)} = \left[N_1^{(\tau)} \quad N_2^{(\tau)} \quad N_{12}^{(\tau)} \quad N_{21}^{(\tau)} \quad T_1^{(\tau)} \quad T_2^{(\tau)} \quad P_1^{(\tau)} \quad P_2^{(\tau)} \quad S_3^{(\tau)} \right]^T \tag{29}$$

and it is connected with the τ -th order generalized displacements according to the following equation given in compact form

$$\mathbf{S}^{(\tau)} = \sum_{\eta=0}^{N+1} \mathbf{A}^{(\tau\eta)} \mathbf{D}_\Omega \mathbf{u}^{(\eta)} \tag{30}$$

where $\tau = 0,1,2,...,N,N+1$. The term $\mathbf{A}^{(\tau\eta)}$, for $\tau,\eta = 0,1,2,...,N,N+1$, is the stiffness matrix and it is explicitly given for a generic laminated composite shell embedding l orthotropic elastic layers in [61]. In this work, the stiffness terms $\bar{B}_{nm}^{(k)}$ are defined as:

$$\begin{aligned} \bar{B}_{nm}^{(k)} &= \bar{E}_{nm}^{(k)} \quad \text{for} \quad n,m = 1,2,3,6 \\ \bar{B}_{nm}^{(k)} &= \kappa \bar{E}_{nm}^{(k)} \quad \text{for} \quad n,m = 4,5 \end{aligned} \tag{31}$$

Terms $\bar{E}_{nm}^{(k)}$ are employed to specify the elastic constants and they depend on the mechanical properties of the structure. This general notation permits the definition of both reduced elastic coefficients ($\bar{E}_{nm}^{(k)} = \bar{Q}_{nm}^{(k)}$) or the classical ones ($\bar{E}_{nm}^{(k)} = \bar{C}_{nm}^{(k)}$) depending on the employed kinematic model [61]. The reduced stiffness values must be used for kinematic models with constant or linear transverse normal displacement through the thickness, while the classical ones must be employed for those kinematic models with at least a quadratic displacement form through the thickness. Similar considerations can be made for the shear correction factor $\kappa = 1/\chi$. It is equal to the constant value of $5/6$ (that means $\chi = 1.2$) in the case of a structural theory which considers a non-parabolic shear stress through the thickness. In the other cases, this factor is neglected. The HSDTs here developed do not use the shear correction factor. The Generalized Integral Quadrature (GIQ) technique can be used for the integrals proposed in the present formulation [61].

The Hamilton's principle allows to obtain the equilibrium governing equations

$$\mathbf{D}_\Omega^* \mathbf{S}^{(\tau)} + \mathbf{q}^{(\tau)} = \mathbf{0} \tag{32}$$

This expression is general for a defined order $\tau = 0,1,2,...,N,N+1$ used in the kinematic expansion. The equilibrium differential operator $\mathbf{D}_\Omega^*$ has the explicit form defined in [61]. $\mathbf{q}^{(\tau)}$ is the load vector for the forces

applied at the external surfaces of the structure. Three load components for each order $\tau = 0,1,2,...,N,N+1$ can be included

$$\mathbf{q}^{(\tau)} = \begin{bmatrix} q_1^{(\tau)} & q_2^{(\tau)} & q_n^{(\tau)} \end{bmatrix}^T \tag{33}$$

The considered shells are loaded only by external pressures along the principal curvilinear coordinate directions, on the top surface $q_1^{(+)}, q_2^{(+)}, q_n^{(+)}$ and on the bottom one $q_1^{(-)}, q_2^{(-)}, q_n^{(-)}$. The external forces in generalized form are

$$\begin{aligned} q_1^{(\tau)} &= q_1^{(-)} F_\tau^{(-)} H_1^{(-)} H_2^{(-)} + q_1^{(+)} F_\tau^{(+)} H_1^{(+)} H_2^{(+)} \\ q_2^{(\tau)} &= q_{2a}^{(-)} F_\tau^{(-)} H_1^{(-)} H_2^{(-)} + q_{2a}^{(+)} F_\tau^{(+)} H_1^{(+)} H_2^{(+)} \\ q_n^{(\tau)} &= q_n^{(-)} F_\tau^{(-)} H_1^{(-)} H_2^{(-)} + q_n^{(+)} F_\tau^{(+)} H_1^{(+)} H_2^{(+)} \end{aligned} \tag{34}$$

The external loads are applied on the outer surfaces, and both the thickness function $F_\tau^{(\pm)}$ and the geometric parameters $H_1^{(\pm)}, H_2^{(\pm)}$ must be evaluated on the external surfaces of the shell. These surfaces are given by $\zeta = \pm h/2$. Therefore, the final system has the following form

$$\sum_{\eta=0}^{N+1} \mathbf{L}^{(\tau\eta)} \mathbf{u}^{(\eta)} + \mathbf{q}^{(\tau)} = \mathbf{0} \tag{35}$$

The Eq.(35) is valid for each order $\tau = 0,1,2,...,N,N+1$ of the kinematic expansion and it is defined as the fundamental nucleus of the Carrera Unified Formulation [61]. The fundamental operator $\mathbf{L}^{(\tau\eta)} = \mathbf{D}_\Omega^* \mathbf{A}^{(\tau\eta)} \mathbf{D}_\Omega$, for $\tau, \eta = 0,1,2,...,N,N+1$, is defined as

$$\mathbf{L}^{(\tau\eta)} = \begin{bmatrix} L_{11}^{(\tau\eta)} & L_{12}^{(\tau\eta)} & L_{13}^{(\tau\eta)} \\ L_{21}^{(\tau\eta)} & L_{22}^{(\tau\eta)} & L_{23}^{(\tau\eta)} \\ L_{31}^{(\tau\eta)} & L_{32}^{(\tau\eta)} & L_{33}^{(\tau\eta)} \end{bmatrix} \tag{36}$$

Each term $L_{fg}^{(\tau\eta)}$ is defined in [61] for $f, g = 1,2,3$ and $\tau, \eta = 0,1,2,...,N,N+1$ of the fundamental operator. The fundamental system has $3 \times (N+2)$ equilibrium equations for a generic order of kinematic expansion. The appropriate boundary conditions must be imposed to solve the static problem. In the numerical applications, clamped (C), simply-supported (S) and free (F) edges can be considered. All the details how to impose these conditions in the formulation above presented were detailed in [61].

Higher-order Layer Wise (LW) kinematic models can be obtained from the ESL ones proposed in Eq.(25) simply considering the dependence of the displacement from the k-th layer and using a combination of

Legendre polynomials as thickness functions. Several details about LW theories can be found in [61]. The employed acronyms for these theories are LD1-LD4 where L indicates the layer wise approach, D specifies that the governing equations are only expressed in terms of generalized displacement, 1-4 is the order of expansion through the thickness.

3.1 Numerical Solution

The system of governing equations presented in the previous section is numerically solved by means of the Generalized Differential Quadrature (GDQ) method (see details in the review paper [5]). The GDQ method permits the evaluation of the derivative of a function for each point of the domain. In the proposed models, the Chebyshev-Gauss-Lobatto grid distribution is used as reported above. Therefore, the structural problems become two-dimensional, and the grid distribution must be employed along the two principal curvilinear coordinates α_1, α_2. The total number of grid points must be separately defined for each principal direction. $T = I_N$ indicates the number of points along α_1, whereas $T = I_M$ is that for the other coordinate α_2. The GIQ method uses the same ideas of the GDQ technique, as demonstrated in [5]. The static problem is then numerically solved. The fundamental equilibrium equations and the related boundary conditions are given in numerical form by means of the GDQ method. Therefore, the fundamental system (35) can be written as

$$\mathbf{K}\boldsymbol{\delta} = \mathbf{f} \tag{37}$$

where $\mathbf{K}$ is the stiffness matrix, $\boldsymbol{\delta}$ is the displacement vector, and $\mathbf{f}$ is the external load vector. Equation (37) is an algebraic linear problem. The static condensation allows the reduction of the problem size using a separation between the degrees of freedom of the inner points of the domain (*d*) and those linked to the boundaries (*b*). Consequently, the new system becomes

$$\begin{aligned} \mathbf{K}_{bb}\boldsymbol{\delta}_b + \mathbf{K}_{bd}\boldsymbol{\delta}_d &= \mathbf{f}_b \\ \mathbf{K}_{db}\boldsymbol{\delta}_b + \mathbf{K}_{dd}\boldsymbol{\delta}_d &= \mathbf{f}_d \end{aligned} \tag{38}$$

where the vector of the degrees of freedom related to the boundary $\boldsymbol{\delta}_b$ is defined as

$$\boldsymbol{\delta}_b = \mathbf{K}_{bb}^{-1}\left(\mathbf{f}_b - \mathbf{K}_{bd}\boldsymbol{\delta}_d\right) \tag{39}$$

The substitution of equation (39) in equation (38) proposes the final algebraic system including the unknown variable vector $\boldsymbol{\delta}_d$

$$\left(\mathbf{K}_{dd} - \mathbf{K}_{db}\mathbf{K}_{bb}^{-1}\mathbf{K}_{bd}\right)\boldsymbol{\delta}_d = \mathbf{f}_d - \mathbf{K}_{db}\mathbf{K}_{bb}^{-1}\mathbf{f}_b \tag{40}$$

In Eq.(40), the generalized displacements for each order of kinematic expansion are employed.

3.2 Strain and Stress Recovery Method

The proposed shell theories of the present section 3 are two-dimensional models. For this reason, a posteriori recovery procedure, using the three-dimensional elasticity theory [61], allows to obtain the effective shear and normal stresses through the thickness of the structure. The 3D equilibrium equations for shells rearranged for this purpose are

$$\begin{aligned}&\frac{\partial \tau_{13}}{\partial \zeta}+\tau_{13}\left(\frac{2}{R_1+\zeta}+\frac{1}{R_2+\zeta}\right)=\\&=-\frac{1}{A_1\left(1+\zeta/R_1\right)}\frac{\partial \sigma_1}{\partial \alpha_1}+\frac{\sigma_2-\sigma_1}{A_1A_2\left(1+\zeta/R_2\right)}\frac{\partial A_2}{\partial \alpha_1}+\\&-\frac{1}{A_2\left(1+\zeta/R_2\right)}\frac{\partial \tau_{12}}{\partial \alpha_2}-\frac{2\tau_{12}}{A_1A_2\left(1+\zeta/R_1\right)}\frac{\partial A_1}{\partial \alpha_2}\end{aligned} \tag{41}$$

$$\begin{aligned}&\frac{\partial \tau_{23}}{\partial \zeta}+\tau_{23}\left(\frac{1}{R_1+\zeta}+\frac{2}{R_2+\zeta}\right)=\\&=-\frac{1}{A_2\left(1+\zeta/R_2\right)}\frac{\partial \sigma_2}{\partial \alpha_2}+\frac{\sigma_1-\sigma_2}{A_1A_2\left(1+\zeta/R_1\right)}\frac{\partial A_1}{\partial \alpha_2}+\\&-\frac{1}{A_1\left(1+\zeta/R_1\right)}\frac{\partial \tau_{12}}{\partial \alpha_1}-\frac{2\tau_{12}}{A_1A_2\left(1+\zeta/R_2\right)}\frac{\partial A_2}{\partial \alpha_1}\end{aligned} \tag{42}$$

$$\begin{aligned}&\frac{\partial \sigma_3}{\partial \zeta}+\sigma_3\left(\frac{1}{R_1+\zeta}+\frac{1}{R_2+\zeta}\right)=\\&=-\frac{1}{A_1\left(1+\zeta/R_1\right)}\frac{\partial \tau_{13}}{\partial \alpha_1}-\frac{\tau_{13}}{A_1A_2\left(1+\zeta/R_2\right)}\frac{\partial A_2}{\partial \alpha_1}+\\&-\frac{1}{A_2\left(1+\zeta/R_2\right)}\frac{\partial \tau_{23}}{\partial \alpha_2}-\frac{\tau_{23}}{A_1A_2\left(1+\zeta/R_1\right)}\frac{\partial A_1}{\partial \alpha_2}+\frac{\sigma_1}{R_1+\zeta}+\frac{\sigma_2}{R_2+\zeta}\end{aligned} \tag{43}$$

Eqs. (41)-(43) must be used in discrete form in order to be evaluated in each point of the three-dimensional shell [61]. The GDQ method is employed in the discrete system in each point $\left(\alpha_{1i},\alpha_{2j}\right)$ of the reference surface of the shell

$$\begin{aligned}&\sum_{k=1}^{I_T}\varsigma_{mk}^{\zeta(1)}\tau_{13(ijk)}+\tau_{13(ijm)}\left(\frac{2}{R_{1(ij)}+\zeta_m}+\frac{1}{R_{2(ij)}+\zeta_m}\right)=\\&=-\frac{1}{A_{1(ij)}\left(1+\zeta_m/R_{1(ij)}\right)}\frac{\partial \sigma_1}{\partial \alpha_1}\bigg|_{(ijm)}+\frac{\sigma_{2(ijm)}-\sigma_{1(ijm)}}{A_{1(ij)}A_{2(ij)}\left(1+\zeta_m/R_{2(ij)}\right)}\frac{\partial A_2}{\partial \alpha_1}\bigg|_{(ij)}+\\&-\frac{1}{A_{2(ij)}\left(1+\zeta_m/R_{2(ij)}\right)}\frac{\partial \tau_{12}}{\partial \alpha_2}\bigg|_{(ijm)}-\frac{2\tau_{12(ijm)}}{A_{1(ij)}A_{2(ij)}\left(1+\zeta_m/R_{1(ij)}\right)}\frac{\partial A_1}{\partial \alpha_2}\bigg|_{(ij)}\end{aligned} \tag{44}$$

$$\sum_{k=1}^{I_T}\varsigma_{mk}^{\zeta(1)}\tau_{23(ijk)}+\tau_{23(ijm)}\left(\frac{1}{R_{1(ij)}+\zeta_m}+\frac{2}{R_{2(ij)}+\zeta_m}\right)=$$
$$=-\frac{1}{A_{2(ij)}\left(1+\zeta_m/R_{2(ij)}\right)}\frac{\partial\sigma_2}{\partial\alpha_2}\bigg|_{(ijm)}+\frac{\sigma_{1(ijm)}-\sigma_{2(ijm)}}{A_{1(ij)}A_{2(ij)}\left(1+\zeta_m/R_{1(ij)}\right)}\frac{\partial A_1}{\partial\alpha_2}\bigg|_{(ij)}+ \tag{45}$$
$$-\frac{1}{A_{1(ij)}\left(1+\zeta_m/R_{1(ij)}\right)}\frac{\partial\tau_{12}}{\partial\alpha_1}\bigg|_{(ijm)}-\frac{2\tau_{12(ijm)}}{A_{1(ij)}A_{2(ij)}\left(1+\zeta_m/R_{2(ij)}\right)}\frac{\partial A_2}{\partial\alpha_1}\bigg|_{(ij)}$$

$$\sum_{k=1}^{I_T}\varsigma_{mk}^{\zeta(1)}\sigma_{3(ijk)}+\sigma_{3(ijm)}\left(\frac{1}{R_{1(ij)}+\zeta_m}+\frac{1}{R_{2(ij)}+\zeta_m}\right)=$$
$$=\frac{\sigma_{1(ijm)}}{R_{1(ij)}+\zeta_m}+\frac{\sigma_{2(ijm)}}{R_{2(ij)}+\zeta_m}-\frac{1}{A_{1(ij)}\left(1+\zeta_m/R_{1(ij)}\right)}\frac{\partial\tau_{13}}{\partial\alpha_1}\bigg|_{(ijm)}-\frac{\tau_{13(ijm)}}{A_{1(ij)}A_{2(ij)}\left(1+\zeta_m/R_{2(ij)}\right)}\frac{\partial A_2}{\partial\alpha_1}\bigg|_{(ij)}+ \tag{46}$$
$$-\frac{1}{A_{2(ij)}\left(1+\zeta_m/R_{2(ij)}\right)}\frac{\partial\tau_{23}}{\partial\alpha_2}\bigg|_{(ijm)}-\frac{\tau_{23(ijm)}}{A_{1(ij)}A_{2(ij)}\left(1+\zeta_m/R_{1(ij)}\right)}\frac{\partial A_1}{\partial\alpha_2}\bigg|_{(ij)}$$

where $m=1,2,...,I_T$. The Chebyshev-Gauss-Lobatto grid distribution with I_T points allows to discretize the system in the normal direction ζ. In the results proposed in the present paper, the value $I_T=31$ is set for each numerical investigation. The equilibrium relations (41)-(43) can be written in order to have τ_{13} and τ_{23} as unknown variables. These stresses are calculated from the opportune boundary conditions at the bottom (-) and at the top (+)

$$\begin{aligned}\overline{\tau}_{13(ij1)}&=q_{1(ij)}^{(-)}\\ \overline{\tau}_{23(ij1)}&=q_{2(ij)}^{(-)}\end{aligned} \tag{47}$$

$$\begin{aligned}\overline{\tau}_{13(ijI_T)}&=q_{1(ij)}^{(+)}\\ \overline{\tau}_{23(ijI_T)}&=q_{2(ij)}^{(+)}\end{aligned} \tag{48}$$

The shear stresses along the thickness are

$$\tau_{13(ijm)}=\tilde{\tau}_{13(ijm)}+\frac{q_{1(ij)}^{(+)}-\tilde{\tau}_{13(ijI_T)}}{h}\left(\zeta_m+\frac{h}{2}\right) \tag{49}$$

$$\tau_{23(ijm)}=\tilde{\tau}_{23(ijm)}+\frac{q_{2(ij)}^{(+)}-\tilde{\tau}_{23(ijI_T)}}{h}\left(\zeta_m+\frac{h}{2}\right) \tag{50}$$

for $m=2,3,...,I_T$, where $\tilde{\tau}_{13}$ and $\tilde{\tau}_{23}$ are the shear stresses relative to the boundary conditions on the top surface. The third equilibrium equation (43) allows the calculation of the normal stress σ_3, using the opportune boundary conditions on the external shell surfaces

$$\bar{\sigma}_{3(ij1)} = q^{(-)}_{3(ij)}$$
$$\bar{\sigma}_{3(ijI_T)} = q^{(+)}_{3(ij)} \tag{51}$$

The normal stress through the thickness is

$$\sigma_{3(ijm)} = \tilde{\sigma}_{3(ijm)} + \frac{q^{(+)}_{3(ij)} - \tilde{\sigma}_{3(ijI_T)}}{h}\left(\zeta_m + \frac{h}{2}\right) \tag{52}$$

for $m = 2,3,...,I_T$, where $\tilde{\sigma}_3$ is the normal stress imposed at the top as boundary conditions. The shear strains γ_{13}, γ_{23} and the normal strain ε_3 can be calculated using the computed shear stresses τ_{13}, τ_{23} and normal stress σ_3 using the constitutive laws. The strains through the thickness are

$$\gamma_{13(ijm)} = \frac{\bar{C}^{(m)}_{55}\tau_{13(ijm)} - \bar{C}^{(m)}_{45}\tau_{23(ijm)}}{\bar{C}^{(m)}_{55}\bar{C}^{(m)}_{44} - \left(\bar{C}^{(m)}_{45}\right)^2} \tag{53}$$

$$\gamma_{23(ijm)} = \frac{\bar{C}^{(m)}_{44}\tau_{23(ijm)} - \bar{C}^{(m)}_{45}\tau_{13(ijm)}}{\bar{C}^{(m)}_{55}\bar{C}^{(m)}_{44} - \left(\bar{C}^{(m)}_{45}\right)^2} \tag{54}$$

$$\varepsilon_{3(ijm)} = \frac{\sigma_{3(ijm)} - \bar{C}^{(m)}_{13}\varepsilon_{1(ijm)} - \bar{C}^{(m)}_{23}\varepsilon_{2(ijm)} - \bar{C}^{(m)}_{36}\gamma_{12(ijm)}}{\bar{C}^{(m)}_{33}} \tag{55}$$

Equations (54)-(55) do not guarantee the strain compatibility between the different layers, and this feature could give an error.

4. RESULTS

Five different cases are analyzed in this section, the first four ones permit comparisons between the exact 3D shell models proposed in Section 2 and the numerical 2D GDQ solutions proposed in Section 3 because simply supported sides, harmonic forms for displacements, stresses and loads, and cross-ply configurations are considered. The last case is analyzed only by means of 2D GDQ solutions because of more realistic geometries, boundary conditions, lamination schemes and load impositions. The first case is a simply-supported square multilayered composite plate subjected to an harmonic transverse shear load applied at the top. The second case considers the same geometry, boundary conditions and load application of the case 1 but the lamination scheme is a sandwich configuration with two external skins in Titanium Alloy and an internal soft core made of Foam. The third case is a simply supported spherical shell with the same lamination scheme of case 1 (four composite layer configuration with fiber orientation 0/90/0/90) and transverse shear load applied at the top in harmonic

form. The fourth case considers the same geometry, boundary and load conditions of case 3 but for a sandwich configuration with external isotropic skins and internal foam core. The case 5 is a super elliptic panel of revolution with the boundary conditions for the four sides given as Clamped (C)/Free (F)/Clamped (C)/Free (F). The transverse shear load is uniform and applied at the top. The shell is made of four composite layers with lamination scheme 20/35/45/70. A summary of the geometrical data (radii of curvature, in-plane dimensions, global thickness, thickness layers), lamination scheme, and direction, amplitude and half-wave numbers for the applied loads are proposed in Table 1 for the all the five proposed cases. The materials employed in the proposed lamination schemes (both multilayered composite and multilayered sandwich configurations) have elastic properties as summarized in Table 2. Figure 2 shows an exhaustive overview of the geometries employed in the five proposed cases.

Figures 3-6 propose stresses and displacements through the thickness of the case 1 about the simply supported multilayered composite plates subjected to an harmonic transverse shear load at the top. Figures 3 and 4 give information about the stress and displacement evaluations through the thickness of the thick plate (a/h=10). Figures 5 and 6 propose the same quantities through the thickness for the thin plate case (a/h=100). In these figures, "3D EM" means the closed form 3D shell solution where differential equations in z are solved by means of the Exponential Matrix method, "3D GDQ" is the closed form 3D shell solution where differential equations in z are solved by means of the GDQ method. All the other theories are 2D GDQ shell models implemented in numerical form, in particular "LD4" is a layer wise model with fourth order of expansion for all the displacement components, "ED4" is an equivalent single layer model with fourth order of expansion for all the displacement components, "EDZ4" considers the inclusion of the Murakami's zigzag function in the ED4 model, "TSDT" is a Third order Shear Deformation Theory, "FSDT" is a First order Shear Deformation Theory and "KL" means Kirchhoff-Love 2D model. In all Figures 3-6, 3D EM and 3D GDQ models are always coincident for each thickness ratio and investigated variable. This feature demonstrates the correctness of the new proposed 3D GDQ model with respect to the well-known 3D EM model already validated in past first author's works. Both 3D EM and 3D GDQ models guarantee the correct load boundary conditions in the evaluation of the transverse stresses, the zigzag form of displacements typical of multilayered anisotropic structures, the correct imposition of compatibility conditions for displacements and equilibrium conditions for transverse stresses at each layer interface. Therefore, they are the best solutions for the analysis of multilayered anisotropic structures, but they have the main limitations typical of closed form solutions (simply supported sides, harmonic forms of

displacements, stresses and loads, cross-ply lamination scheme). For these reasons, it is fundamental the validation of new refined 2D GDQ models. These last ones allow to overcome the limitations typical of closed form solutions. LD4 and EDZ4 models are always very close to 3D solutions for each thickness ratio and investigated variable (see Figures 3-6). TSDT, FSDT and KL models exhibit some difficulties because they are classical 2D theories originally developed for classical laminations. ED4 is a refined model but sometimes it exhibits some difficulties (in particular for thick plates) when, for example, the evaluation of typical zigzag form of displacements is necessary. EDZ4 model overcomes this main limitation of ED4 model by means of the use of the Murakami's zigzag function.

All the same theories are employed in the case 2 of Figures 7-10 in order to verify the same conclusions obtained for the simply supported multilayered composite plates of Figures 3-6 when the lamination scheme is changed in a sandwich configuration with Titanium Alloy skins and a soft Foam core. In this case, all the layers are isotropic and therefore there is not an in-plane anisotropy. However, the use of a very soft core gives an important transverse anisotropy because of the different elastic properties between the core and the skins. However, the 3D closed-form solutions are still the best possibilities. For the 2D GDQ models, the best solutions are the LD4 and the EDZ4 ones which are able to capture the zigzag effects for both thick (a/h=10 in Figures 7 and 8) and thin (a/h=100 in Figures 9 and 10) configurations.

Figures 11-18 are used to investigate the radii of curvature effects in the lamination schemes already presented and discussed in Figures 3-10 for plate cases. For this purpose, Figures 11-14 are related to the case 3 where the lamination scheme of the case 1 about the multilayered composite plate is now used in the case of a simply supported spherical shell. Figures 15-18 show the case 4 where the lamination scheme of the case 2 about the sandwich plate with soft core is extended to the simply supported spherical shell geometry. The inclusion of curvature terms in these cases gives a full coupling between all the displacement components, and this feature generates very complicated displacement and stress evaluations through the thickness direction. In spite of this feature, 3D shell models still continue to work very well. 2D GDQ models exhibit some difficulties but the use of 3D equilibrium equations, to obtain the "a posteriori" stresses, is very useful to reduce these problems. However, LD4 and EDZ4 models remain the best possible 2D numerical models for the correct displacement and stress analysis of multilayered composite and sandwich spherical shells. The layer wise approach and the Murakami's zigzag function opportunely added in the ESL models allow a quasi-3D reconstruction of all the displacement and stress components through the thickness direction. In these shell cases, EDZ4 model appears to

better work with respect to the LD4 model because of some small numerical problems due to the layer wise assembling procedure connected with curved boundary conditions. However, the LD4 model remains more accurate than ED4, TSDT, FSDT and KL models.

Figures 19 and 20 show the six stress components and the three displacement components for the case 5 about the four layered composite super elliptic panel of revolution subjected to a uniform transverse shear load at the top. Only numerical 2D models are proposed in Figures 19 and 20 because boundary conditions are different from the simply supported ones, and lamination schemes are different from the cross-ply ones. Moreover, a uniform load is applied. This benchmark is very useful for those scientists interested in the development of numerical shell models to understand the correctness of their implementations in the case of more realistic analyses. The best results proposed in Figures 19 and 20 are those obtained via LD4 and EDZ4 models.

5. CONCLUSIONS

This work proposes 3D analytical/semi-analytical and 2D numerical GDQ shell models for the static analysis of multilayered composite and sandwich structures when they are subjected to transverse shear loads. Investigated geometries are simply supported plates and spherical shells in order to compare closed form solutions with numerical 2D methods. More complicated geometries with boundary conditions different from the simple supported ones and loads different from the harmonic ones are also investigated by means of only 2D numerical GDQ shell models. The two presented 3D shell models, based on the exponential matrix method and on the GDQ method for the solution of differential equations in z, are always coincident for each geometry, thickness ratio, lamination scheme, material and load. Moreover, they are able to correctly describe the multilayered anisotropic structures giving the zigzag effect of displacements and the fulfillment of the interlaminar and load boundary conditions. 2D GDQ models overcome the main limitations of 3D closed form solutions, and they allow the investigation of more realistic cases in terms of geometries, boundary conditions and applied loads. For the 2D GDQ models, the LD4 model (based on a fourth order layer wise approach) and the EDZ4 model (based on a fourth order equivalent single layer approach including the Murakami's zigzag function) are those which are more refined, with a quasi-3D behavior for each investigated case and variable. The use of 3D elasticity equations to "a posteriori" recover the transverse stresses in 2D GDQ models allows an important improvement in the evaluation of such variables through the thickness. This last feature is valid for all the presented 2D GDQ shell models (both classical and refined ones).

REFERENCES

[1] J.N. Reddy, Mechanics of Laminated Composite Plates and Shells. Theory and Analysis. Second Edition, CRC Press, New York, 2004.

[2] S.W. Tsai, Composites Design, Think Composites, Dayton OH, 1987.

[3] J.R. Vinson, The Behavior of Sandwich Structures of Isotropic and Composite Materials, Technomic Publishing Company, Inc., Lancaster, Pennsylvania USA, 1999.

[4] C. Shu, Differential quadrature and its application in engineering, Springer, London, 2000.

[5] F. Tornabene, F. Fantuzzi, F. Ubertini and E. Viola, Strong formulation finite element method based on differential quadrature: a survey. Applied Mechanics Review, 67, 020801 (55 pages), 2015.

[6] F. Tornabene and F. Fantuzzi, Strong formulation isogeometric analysis (SFIGA) for laminated composite arbitrarily shaped plates, Composites. Part B, Engineering, 96, 173-203, 2016.

[7] F. Tornabene, F. Fantuzzi, M. Bacciocchi, A.M.A. Neves and A.J.M. Ferreira, MLSDQ based on RBFs for the free vibrations of laminated composite doubly-curved shells, Composites. Part B, Engineering, 99, 30-47, 2016.

[8] N. Fantuzzi, R. Dimitri and F. Tornabene, A SFEM-based evaluation of Mode-I stress intensity factor in composite structures, Composite Structures, 145, 162-185, 2016.

[9] F. Tornabene, R. Dimitri and E. Viola, Transient dynamic response of generally shaped arches based on a GDQ-Time-stepping method, International Journal of Mechanical Sciences, 114, 277-314, 2016.

[10] R. Dimitri, N. Fantuzzi, F. Tornabene and G. Zavarise, Innovative numerical methods based on SFEM and IGA for computing stress concentrations in isotropic plates with discontinuities, International Journal of Mechanical Sciences, 118, 166-187, 2016.

[11] H. Kurtaran, Geometrically nonlinear transient analysis of moderately thick laminated composite shallow shells with generalized differential quadrature method, Composite Structures, 125, 605-614, 2015.

[12] M.A. De Rosa and M. Lippiello, Nonlocal frequency analysis of embedded single-walled carbon nanotube using the Differential Quadrature Method, Composites. Part B, Engineering, 84, 41-51, 2016.

[13] F. Mehralian and Y.T. Beni, Size-dependent torsional buckling analysis of functionally graded cylindrical shell, Composites. Part B, Engineering, 94, 11-25, 2016.

[14] R. Ansari, J. Torabi and M.F. Shojaei, Buckling and vibration analysis of embedded functionally graded carbon nanotube-reinforced composite annular sector plates under thermal loading, Composites. Part B, Engineering, 109, 197-213, 2017.

[15] M. Mohammadimeh and S. Shahedi, High-order buckling and free vibration analysis of two types sandwich beam including AL or PVC-foam flexible core and CNTs reinforced nanocomposite face sheets using GDQM, Composites. Part B, Engineering, 108, 91-107, 2017.

[16] E. Viola, F. Tornabene and N. Fantuzzi, General higher-order shear deformation theories for the free vibration analysis of completely doubly-curved laminated shells and panels, Composite Structures, 95, 639-666, 2013.

[17] E. Viola, F. Tornabene and N. Fantuzzi, Static analysis of completely doubly-curved laminated shells and panels using general higher-order shear deformation theories, Composite Structures, 101, 59-93, 2013.

[18] F. Tornabene, E. Viola and N. Fantuzzi, General higher-order equivalent single layer theory for free vibrations of doubly-curved laminated composite shells and panels, Composite Structures, 104, 94-117, 2013.

[19] E. Carrera, Theories and finite elements for multilayered, anisotropic, composite plates and shells, Archives of Computational Methods in Engineering, 9, 87-140, 2002.

[20] E. Carrera, On the use of the Murakami's zig-zag function in the modeling of layered plates and shells, Computers and Structures, 82, 541-554, 2002.

[21] F. Tornabene, N. Fantuzzi, E. Viola and E. Carrera, Static analysis of doubly-curved anisotropic shells and panels using CUF approach, differential geometry and differential quadrature method, Composite Structures, 107, 675-697, 2014.

[22] F. Tornabene, A. Liverani and G. Caligiana, Laminated composite rectangular and annular plates: A GDQ solution for static analysis with a posteriori shear and normal stress recovery, Composites. Part B, engineering, 43, 1847-1872, 2012.

[23] F. Tornabene and E. Viola, Static analysis of functionally graded doubly-curved shells and panels of revolution, Meccanica 48, 901-930, 2013.

[24] E. Viola, F. Tornabene and N. Fantuzzi, Static analysis of completely doubly-curved laminated shells and panels using general higher-order shear deformation theories, Composite Structures 101, 59-93, 2013.

[25] N.J. Pagano, Exact solutions for composite laminates in cylindrical bending, Journal of Composite Materials, 3, 398-411, 1969.
[26] N.J. Pagano, Exact solutions for rectangular bidirectional composites and sandwich plates, Journal of Composite Materials, 4, 20-34, 1970.
[27] N.J. Pagano and A.S.D. Wang, Further study of composite laminates under cylindrical bending, Journal of Composite Materials, 5, 521-528, 1971.
[28] Y. Xu and D. Zhou, Three-dimensional elasticity solution of functionally graded rectangular plates with variable thickness, Composite Structures, 91, 56-65, 2009.
[29] H.-R. Meyer-Piening, Application of the elasticity solution to linear sandwich beam, plate and shell analyses, Journal of Sandwich Structures and Materials, 6, 295-312, 2004.
[30] L. Demasi, Three-dimensional closed form solutions and exact thin plate theories for isotropic plates, Composite Structures, 80, 183-195, 2007.
[31] J.G. Ren, Exact solutions for laminated cylindrical shells in cylindrical bending, Composite Science and Technology, 29, 169-187, 1987.
[32] T.K. Varadan and K. Bhaskar, Bending of laminated orthotropic cylindrical shells - an elasticity approach, Composite Structures, 17, 141-156, 1991.
[33] J.-R. Fan and J.-Y. Zhang, Exact solutions for thick laminated shells, Science in China, 35, 1343-1355, 1992.
[34] J.-R. Fan and J.-Y. Zhang, Analytical solutions for thick, doubly curved, laminated shells, Journal of Engineering Mechanics, 118, 1338-1356, 1992.
[35] K.P. Soldatos and J. Ye, Axisymmetric static and dynamic analysis of laminated hollow cylinders composed of monoclinic elastic layers, Journal of Sound and Vibration, 184, 245-259, 1995.
[36] J.-R. Fan and J. Ye, An exact solution for the statics and dynamics of laminated thick plates with orthotropic layers, International Journal of Solids and Structures, 26, 655-662, 1990.
[37] M. Kashtalyan, Three-dimensional elasticity solution for bending of functionally graded rectangular plates, European Journal of Mechanics - A/Solids, 23, 853-864, 2004.
[38] M. Kashtalyan and M. Menshykova, Three-dimensional elasticity solution for sandwich panels with a functionally graded core, Composite Structures, 87, 36-43, 2009.
[39] S.S. Vel and R.C. Batra, Three-dimensional exact solution for the vibration of functionally graded rectangular plates, Journal of Sound and Vibration, 172, 703-730, 2004.
[40] S. Srinivas, A.K. Rao and C.V.J. Rao, Flexure of simply supported thick homogeneous and laminated rectangular plates, Zeitschrift fur Angewandte Mathematik und Mechanik, 49, 449-458, 1969.
[41] A. Messina, Three dimensional free vibration analysis of cross-ply laminated plates through 2D and exact models, 3rd International Conference on Integrity, Reliability and Failure, Porto (Portugal), 20-24 July 2009.
[42] Q. Li, V.P. Iu and K.P. Kou, Three-dimensional vibration analysis of functionally graded material sandwich plates, Journal of Sound and Vibration, 311, 498-515, 2008.
[43] A.E. Armenakas, D.C. Gazis and G. Herrmann, Free Vibrations of Circular Cylindrical Shells, Pergamon Press, Oxford, 1969.
[44] N.N. Huang, Exact analysis for three-dimensional free vibrations of cross-ply cylindrical and doubly-curved laminates, Acta Mechanica, 108, 23-34, 1995.
[45] P. Zahedinejad, P. Malekzadeh, M. Farid and G. Karami, A semi-analytical three-dimensional free vibration analysis of functionally graded curved panels, International Journal of Pressure Vessels and Piping, 87, 470-480, 2010.
[46] P. Malekzadeh, A.R. Fiouz and H. Razi, Three-dimensional dynamic analysis of laminated composite plates subjected to moving load, Composite Structures, 90, 105-114, 2009.
[47] P. Malekzadeh, A. Afsari, P. Zahedinejad and R. Bahadori, Three-dimensional layerwise-finite element free vibration analysis of thick laminated annular plates on elastic foundation, Applied Mathematical Modelling, 34, 776-790, 2010.
[48] P. Malekzadeh, H. Monfared Maharloei and A.R. Vosoughi, A three-dimensional layerwise differential quadrature free vibration of thick skew laminated composite plates, Mechanics of Advanced Materials and Structures, 21, 792-801, 2014.
[49] P. Malekzadeh and M. Ghaedsharaf, Three-dimensional free vibration of laminated cylindrical panels with functionally graded layers, Composite Structures, 108, 894-904, 2014.
[50] P. Malekzadeh and M. Ghaedsharaf, Three-dimensional thermoelastic analysis of finite length laminated cylindrical panels with functionally graded layers, Meccanica, 49, 887-906, 2014.
[51] P. Malekzadeh and Y. Heydarpour, Mixed Navier-layerwise differential quadrature three-dimensional static and free vibration analysis of functionally graded carbon nanotube reinforced composite laminated

plates, Meccanica, 50, 143-167, 2015.
[52] S. Brischetto, Three-dimensional exact free vibration analysis of spherical, cylindrical, and flat one-layered panels, Shock and Vibration, vol.2014, 1-29, 2014.
[53] S. Brischetto, An exact 3D solution for free vibrations of multilayered cross-ply composite and sandwich plates and shells, International Journal of Applied Mechanics, 6, 1-42, 2014.
[54] S. Brischetto, Exact elasticity solution for natural frequencies of functionally graded simply-supported structures, Computer Modeling in Engineering & Sciences, 95, 391-430, 2013.
[55] S. Brischetto, A continuum elastic three-dimensional model for natural frequencies of single-walled carbon nanotubes, Composites. Part B, Engineering, 61, 222-228, 2014.
[56] S. Brischetto, A general exact elastic shell solution for bending analysis of functionally graded structures, Composite Structures, 175, 70-85, 2017.
[57] S. Brischetto, Exact three-dimensional static analysis of single- and multi-layered plates and shells, Composites. Part B, Engineering, 119, 230-252, 2017.
[58] S. Brischetto, A closed-form 3D shell solution for multilayered structures subjected to different load combinations, Aerospace Science and Technology, 70, 29-46, 2017.
[59] S. Brischetto, A 3D layer-wise model for the correct imposition of transverse shear/normal load conditions in FGM shells, International Journal of Mechanical Sciences, 136, 50-66, 2018.
[60] F. Tornabene and S. Brischetto, 3D capability of refined GDQ models for the bending analysis of composite and sandwich plates, spherical and doubly-curved shells, submitted to Thin Walled Structures.
[61] F. Tornabene, N. Fantuzzi, M. Bacciocchi and E. Viola, Laminated Composite Doubly-Curved Shell Structures. Differential Geometry. Higher-order Structural Theories, Esculapio, Bologna, Italy, 2016.

DATA	**CASE 1**	**CASE 2**	**CASE 3**	**CASE 4**	**CASE 5**
$R_1\,[\mathrm{m}]$	∞	∞	10	10	see Figure 2C
$R_2\,[\mathrm{m}]$	∞	∞	10	10	see Figure 2C
$a\,[\mathrm{m}]$	1	1	$\frac{\pi}{4}R_1$	$\frac{\pi}{4}R_1$	see Figure 2C
$b\,[\mathrm{m}]$	1	1	$\frac{\pi}{4}R_2$	$\frac{\pi}{4}R_2$	see Figure 2C
$h\,[\mathrm{m}]$	0.1; 0.01	0.1; 0.01	0.5; 0.1	0.5; 0.1	0.2
$h_1\,[\mathrm{m}]$	$0.25h$	$0.15h$	$0.25h$	$0.15h$	$0.15h$
$h_2\,[\mathrm{m}]$	$0.25h$	$0.7h$	$0.25h$	$0.7h$	$0.35h$
$h_3\,[\mathrm{m}]$	$0.25h$	$0.15h$	$0.25h$	$0.15h$	$0.15h$
$h_4\,[\mathrm{m}]$	$0.25h$	-	$0.25h$	-	$0.35h$
Lamination Scheme	0 / 90 / 0 / 90	Ti22 / Foam / Ti22	0 / 90 / 0 / 90	Ti22 / Foam / Ti22	20 / 35 / 45 / 70
Load	$\mathrm{q}_2^{(+)} = 10000\,\mathrm{Pa}$	$\mathrm{q}_2^{(+)} = 10000\,\mathrm{Pa}$	$\mathrm{q}_2^{(+)} = 10000\,\mathrm{Pa}$	$\mathrm{q}_2^{(+)} = 10000\,\mathrm{Pa}$	$\mathrm{q}_2^{(+)} = -10000\,\mathrm{Pa}$
m	1	1	1	1	UNIFORM
n	1	1	1	1	UNIFORM

Table 1. Geometrical data, lamination schemes and load conditions for the five analyzed cases.

DATA	Composite	Ti22	Foam
$E_1\,[\mathrm{GPa}]$	172	114	0.232
$E_2\,[\mathrm{GPa}]$	6.9	114	0.232
$E_3\,[\mathrm{GPa}]$	6.9	114	0.232
$G_{12}\,[\mathrm{GPa}]$	3.4	$\frac{E}{2(1+\nu)}$	$\frac{E}{2(1+\nu)}$
$G_{13}\,[\mathrm{GPa}]$	3.4	$\frac{E}{2(1+\nu)}$	$\frac{E}{2(1+\nu)}$
$G_{23}\,[\mathrm{GPa}]$	1.4	$\frac{E}{2(1+\nu)}$	$\frac{E}{2(1+\nu)}$
ν_{12}	0.25	0.3	0.2
ν_{13}	0.25	0.3	0.2
ν_{23}	0.25	0.3	0.2

Table 2. Elastic properties of the layers involved in the lamination schemes presented in Table 1.

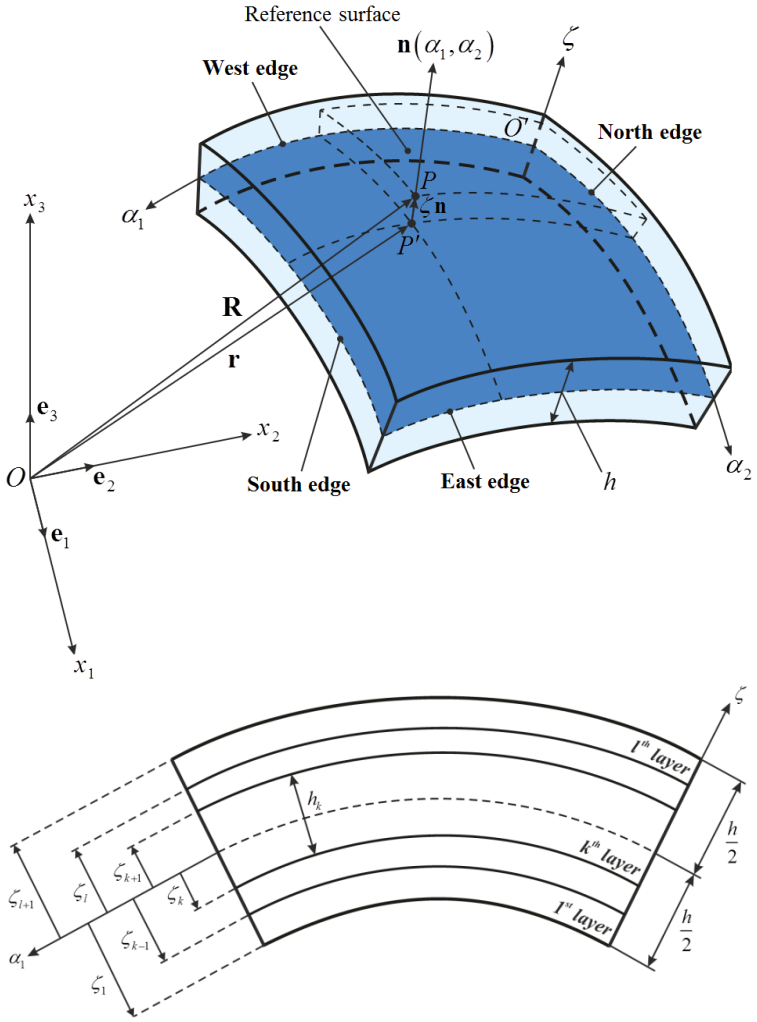

Figure 1. Employed reference systems for a general doubly-curved shell element.

a) Square plate

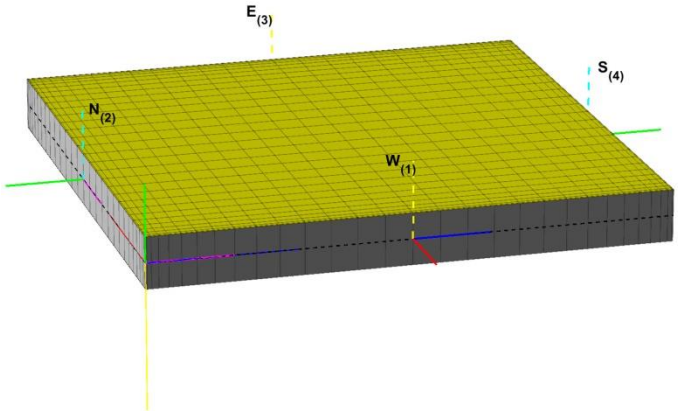

$$\mathbf{r}(s_1, s_2) = s_1\mathbf{e}_1 + s_2\mathbf{e}_2$$
$$s_1 \in [0, a]$$
$$s_2 \in [0, b]$$

b) Spherical Shell Panel

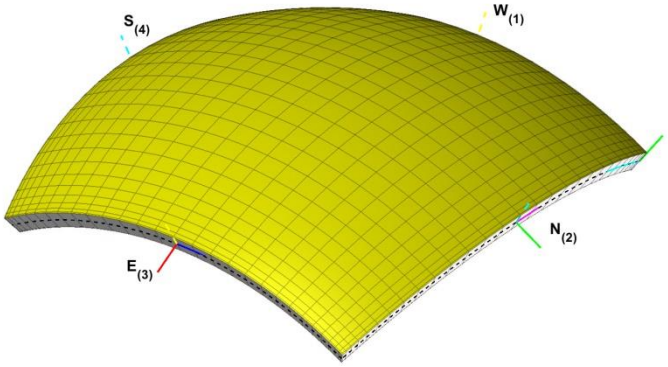

$$\mathbf{r}(\alpha_1, \alpha_2) = R\sin\alpha_1\cos\alpha_2\,\mathbf{e}_1 - R\sin\alpha_1\sin\alpha_2\,\mathbf{e}_2 + \\ + R(1-\cos\alpha_1)\mathbf{e}_3$$
$$\alpha_1 \in [\alpha_1^0, \alpha_1^1], \quad \alpha_2 \in [\alpha_2^0, \alpha_2^1]$$
$$R = R_1 = R_2$$

c) Super Elliptic Panel of Revolution

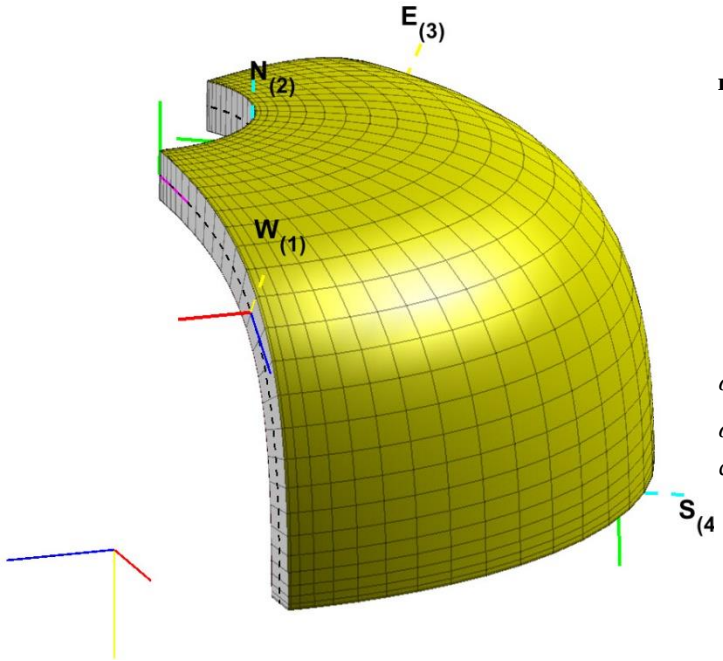

$$\mathbf{r}(\alpha_1, \alpha_2) = \frac{a_1 a_2 \cos\alpha_1}{\left(a_2^n|\cos\alpha_1|^n + a_1^n|\sin\alpha_1|^n\right)^{\frac{1}{n}}}\cos\alpha_2\mathbf{e}_1 + \\ - \frac{a_1 a_2 \cos\alpha_1}{\left(a_2^n|\cos\alpha_1|^n + a_1^n|\sin\alpha_1|^n\right)^{\frac{1}{n}}}\sin\alpha_2\mathbf{e}_2 + \\ + \frac{a_1 a_2 \sin\alpha_1}{\left(a_2^n|\cos\alpha_1|^n + a_1^n|\sin\alpha_1|^n\right)^{\frac{1}{n}}}\mathbf{e}_3$$
$$\alpha_1 \in [\alpha_1^0, \alpha_1^1], \quad \alpha_2 \in [\alpha_2^0, \alpha_2^1]$$
$$\alpha_1^0 = -2\pi/5 \quad \alpha_1^1 = -\pi/18 \quad \alpha_2^0 = 0 \quad \alpha_2^1 = 2\pi/3$$
$$a_1 = 2\text{m} \quad a_2 = 1\text{m} \quad n = 4$$

Figure 2. Geometrical data, GDQ discrete point distribution and local reference system for investigated benchmarks.

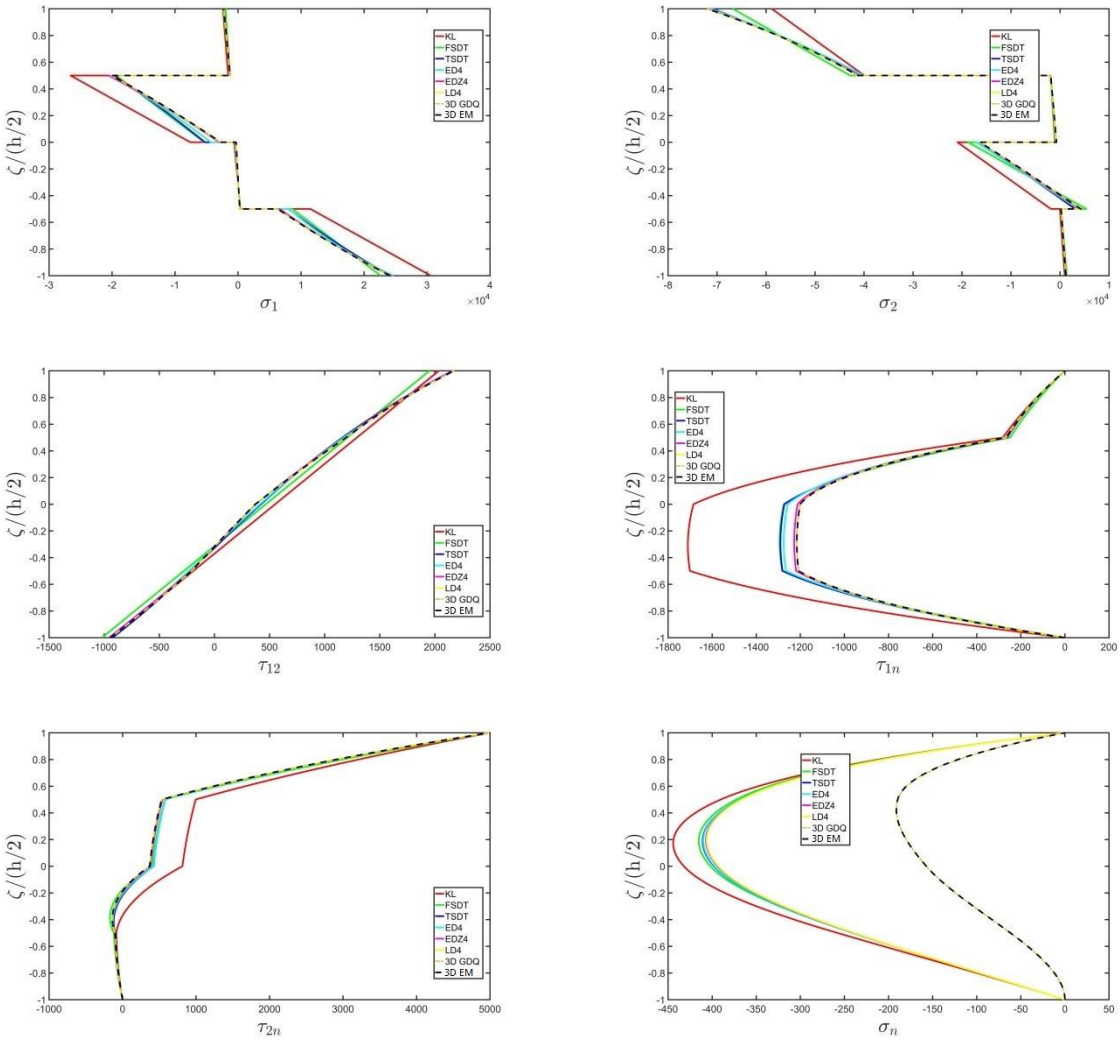

Figure 3. Case 1 $(a/h=10)$: Stress components [Pa] along the thickness direction at the point $P=(0.25a,0.25b)$ for a SSSS square plate made of four composite layers $(0/90/0/90)$ with $h_1=h_2=h_3=h_4=h/4$. Transverse shear sinusoidal pressure $q_2^{(+)}=10000\,\text{Pa}$ $(m=1,n=1)$ at the top surface. Comparison between different structural models.

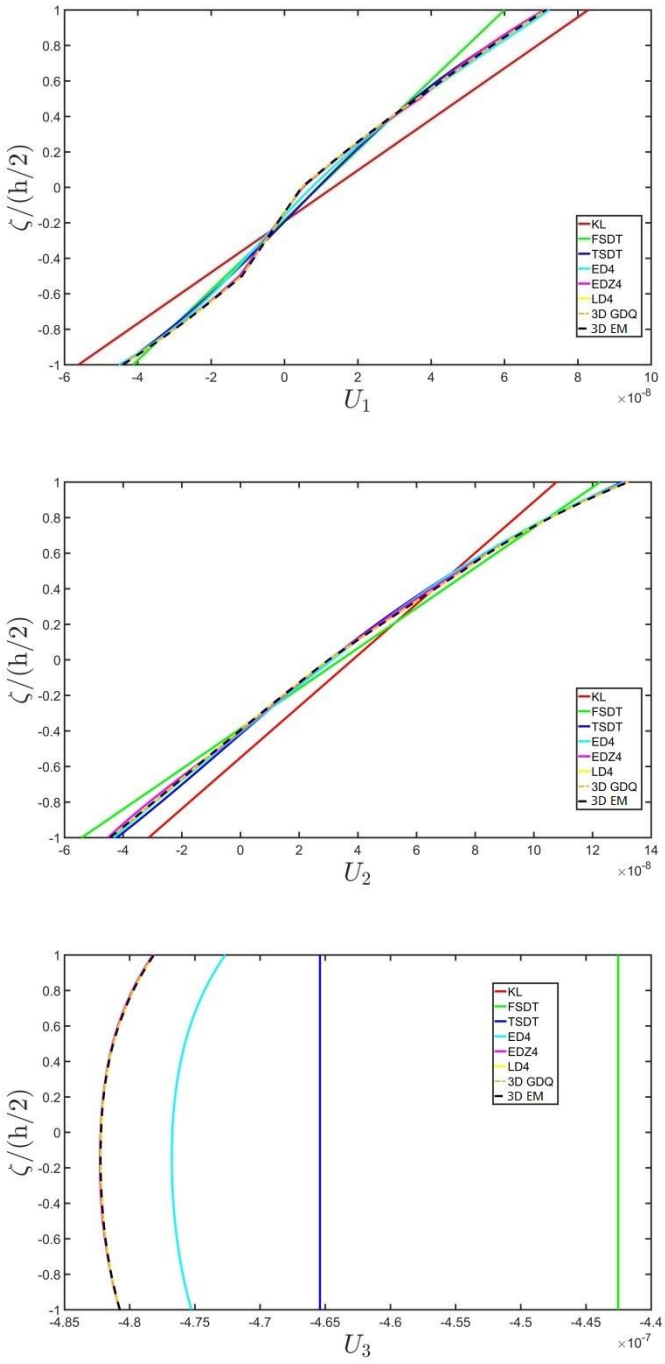

Figure 4. Case 1 $(a/h=10)$: Displacement components [m] along the thickness direction at the point $P=(0.25a, 0.25b)$ for a SSSS square plate made of four composite layers $(0/90/0/90)$ with $h_1=h_2=h_3=h_4=h/4$. Transverse shear sinusoidal pressure $q_2^{(+)}=10000\,\text{Pa}$ $(m=1, n=1)$ at the top surface. Comparison between different structural models.

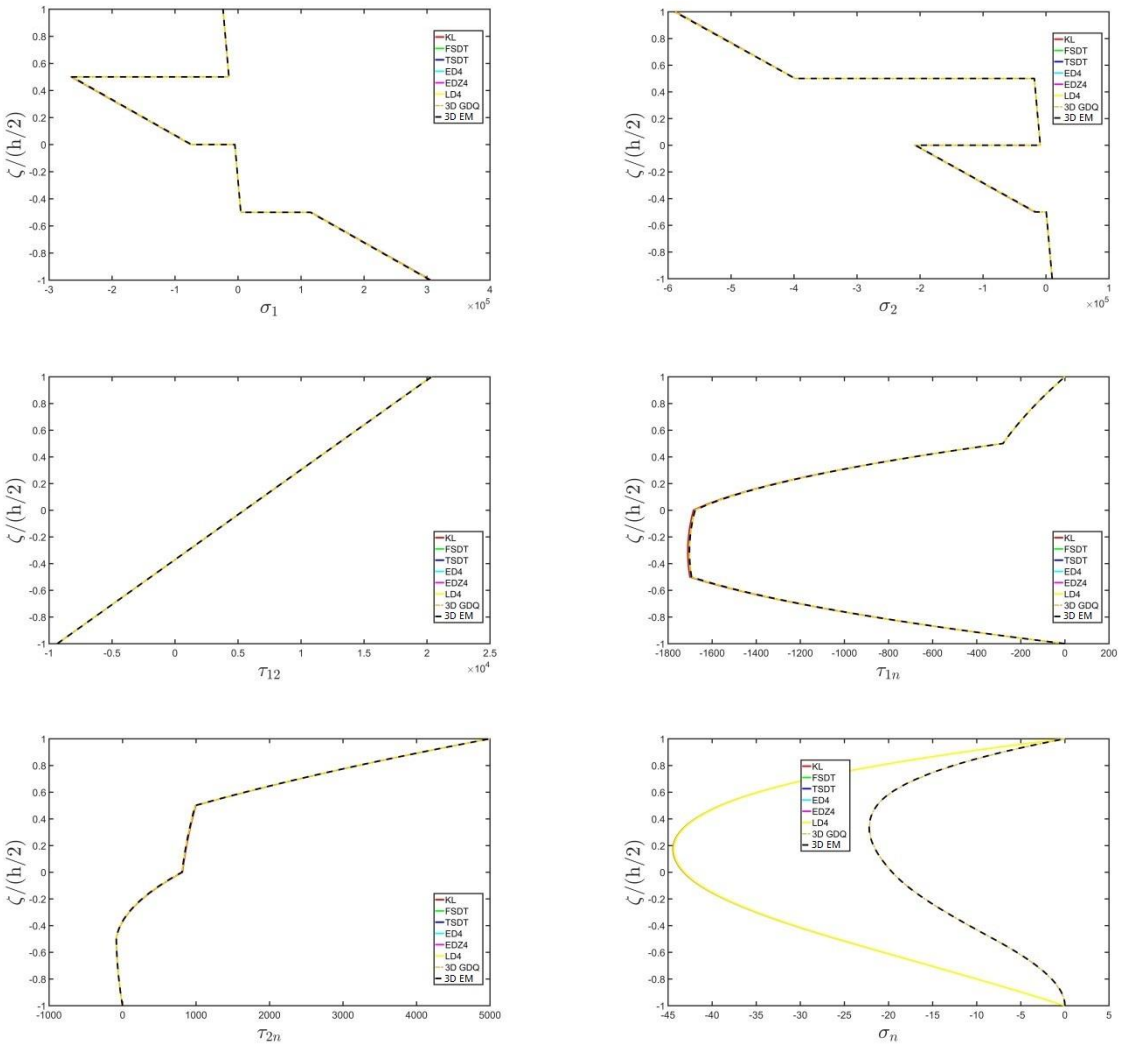

Figure 5. Case 1 $(a/h=100)$: Stress components [Pa] along the thickness direction at the point $P=(0.25a, 0.25b)$ for a SSSS square plate made of four composite layers $(0/90/0/90)$ with $h_1=h_2=h_3=h_4=h/4$. Transverse shear sinusoidal pressure $q_2^{(+)}=10000\,\text{Pa}$ $(m=1, n=1)$ at the top surface. Comparison between different structural models.

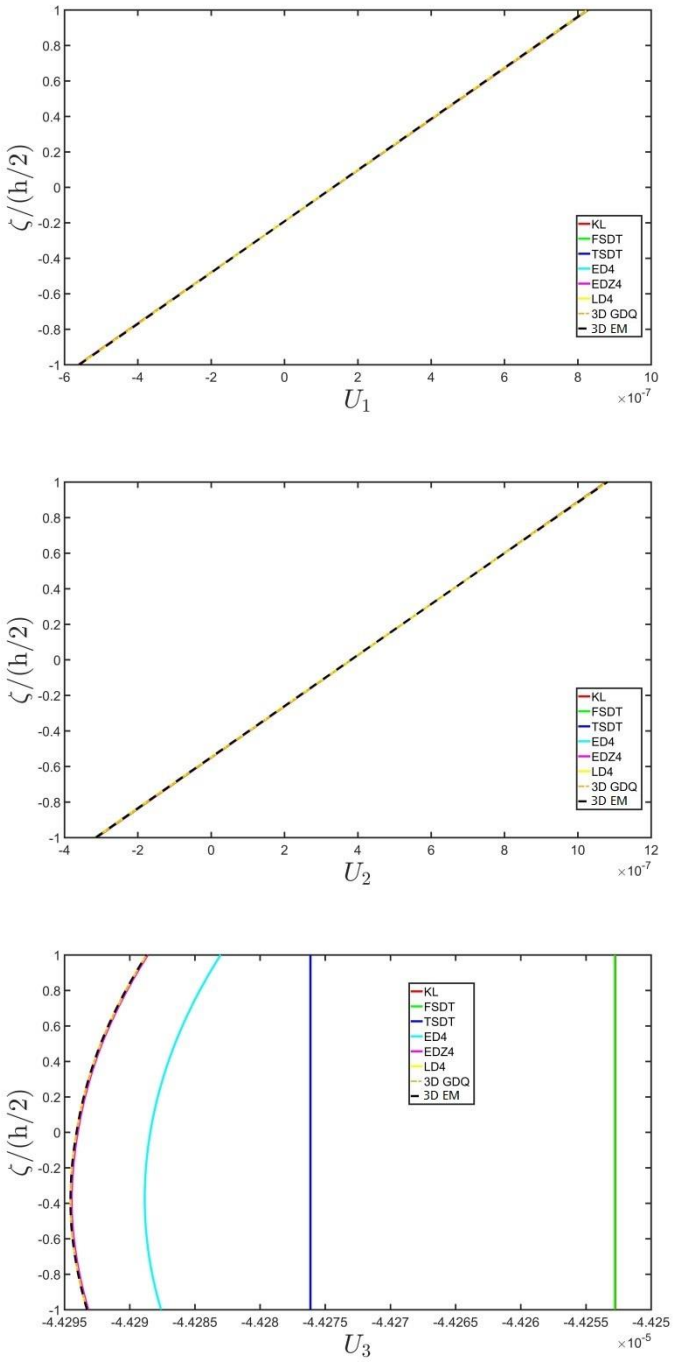

Figure 6. Case 1 $(a/h=100)$: Displacement components [m] along the thickness direction at the point $P=(0.25a,0.25b)$ for a SSSS square plate made of four composite layers $(0/90/0/90)$ with $h_1=h_2=h_3=h_4=h/4$. Transverse shear sinusoidal pressure $q_2^{(+)}=10000\,\text{Pa}$ $(m=1,n=1)$ at the top surface. Comparison between different structural models.

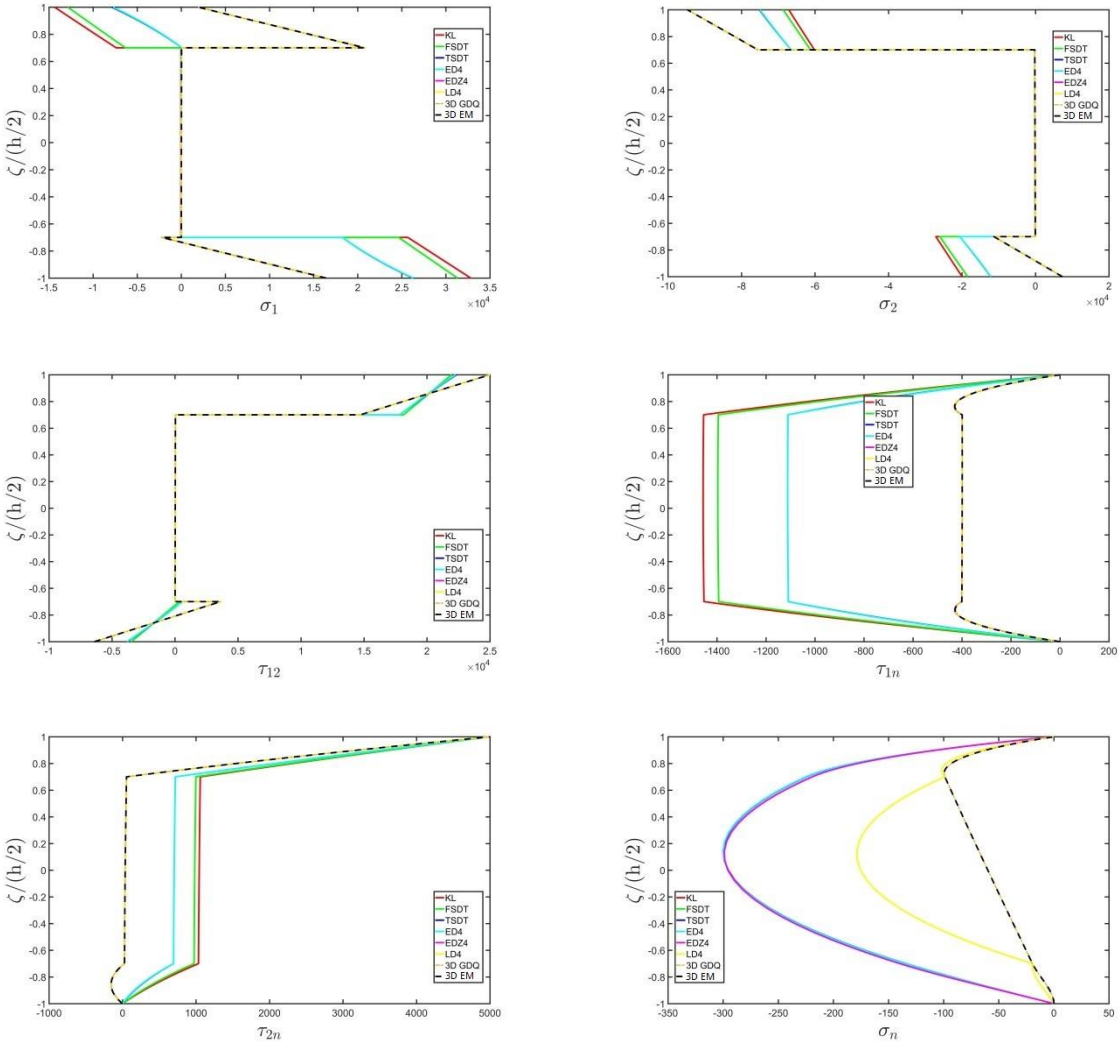

Figure 7. Case 2 $(a/h=10)$: Stress components [Pa] along the thickness direction at the point $P=(0.25a,0.25b)$ for a SSSS square sandwich plate made of three layers $(\text{Titanium Alloy / Foam / Titanium Alloy})$ with $h_1=h_3=0.15h$ and $h_2=0.7h$. Transverse shear sinusoidal pressure $q_2^{(+)}=10000\,\text{Pa}$ $(m=1,n=1)$ at the top surface. Comparison between different structural models.

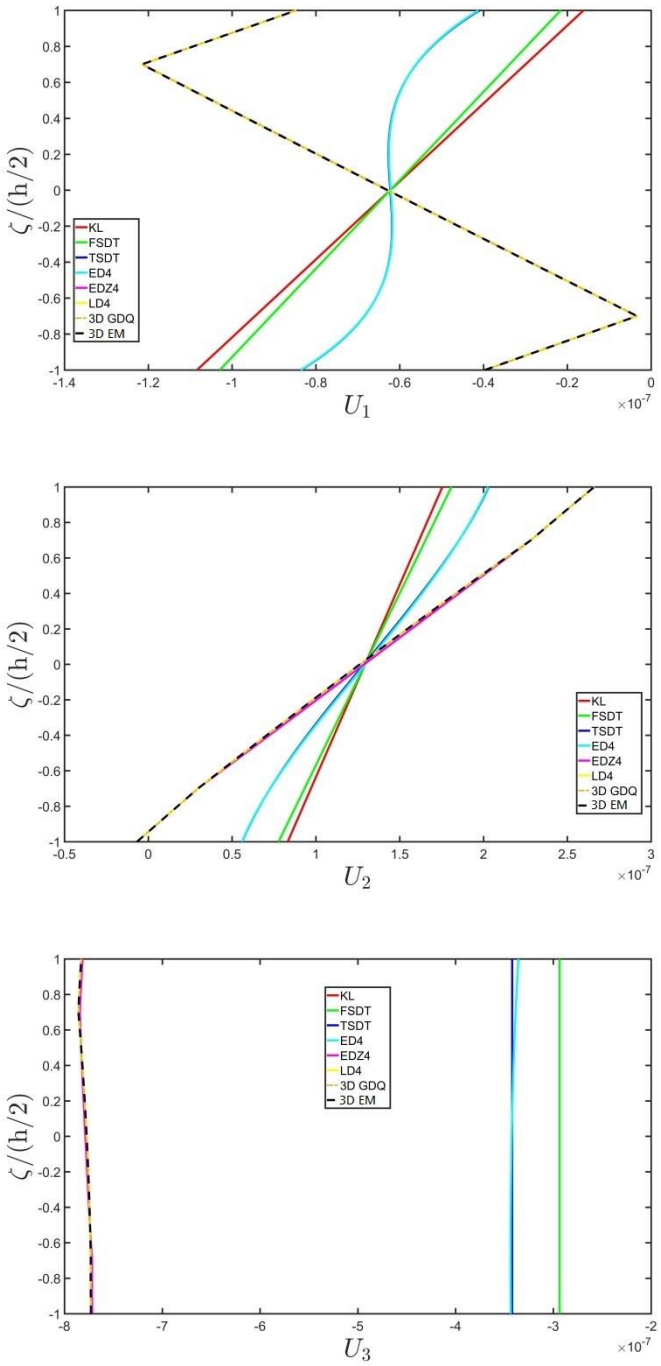

Figure 8. Case 2 $(a/h=10)$: Displacement components [m] along the thickness direction at the point $P=(0.25a,0.25b)$ for a SSSS square sandwich plate made of three layers $(\text{Titanium Alloy / Foam / Titanium Alloy})$ with $h_1=h_3=0.15h$ and $h_2=0.7h$. Transverse shear sinusoidal pressure $q_2^{(+)}=10000\,\text{Pa}$ $(m=1,n=1)$ at the top surface. Comparison between different structural models.

.

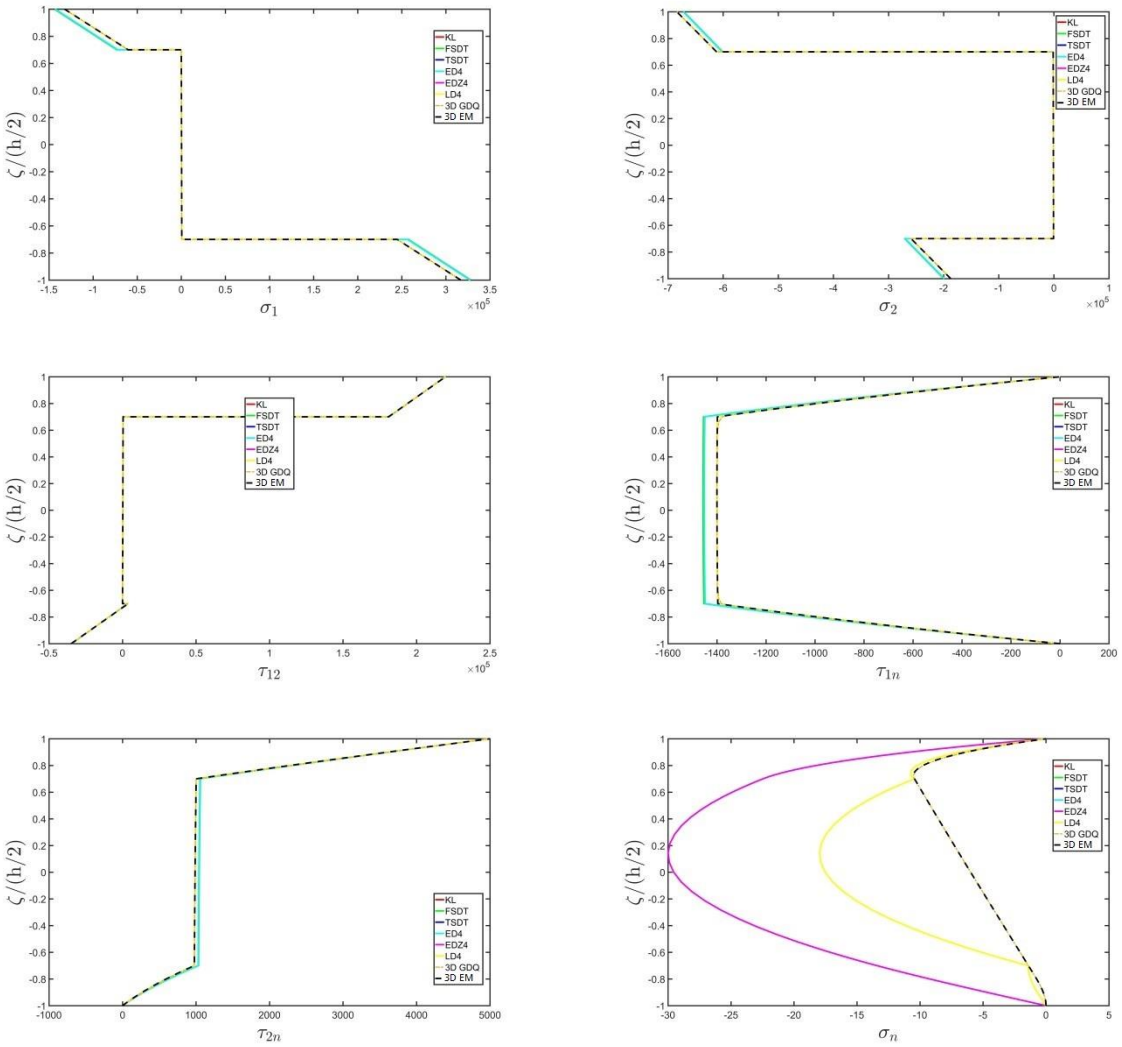

Figure 9. Case 2 $(a/h=100)$: Stress components [Pa] along the thickness direction at the point $P=(0.25a,0.25b)$ for a SSSS square sandwich plate made of three layers $(\text{Titanium Alloy / Foam / Titanium Alloy})$ with $h_1=h_3=0.15h$ and $h_2=0.7h$. Transverse shear sinusoidal pressure $q_2^{(+)}=10000\,\text{Pa}$ $(m=1,n=1)$ at the top surface. Comparison between different structural models.

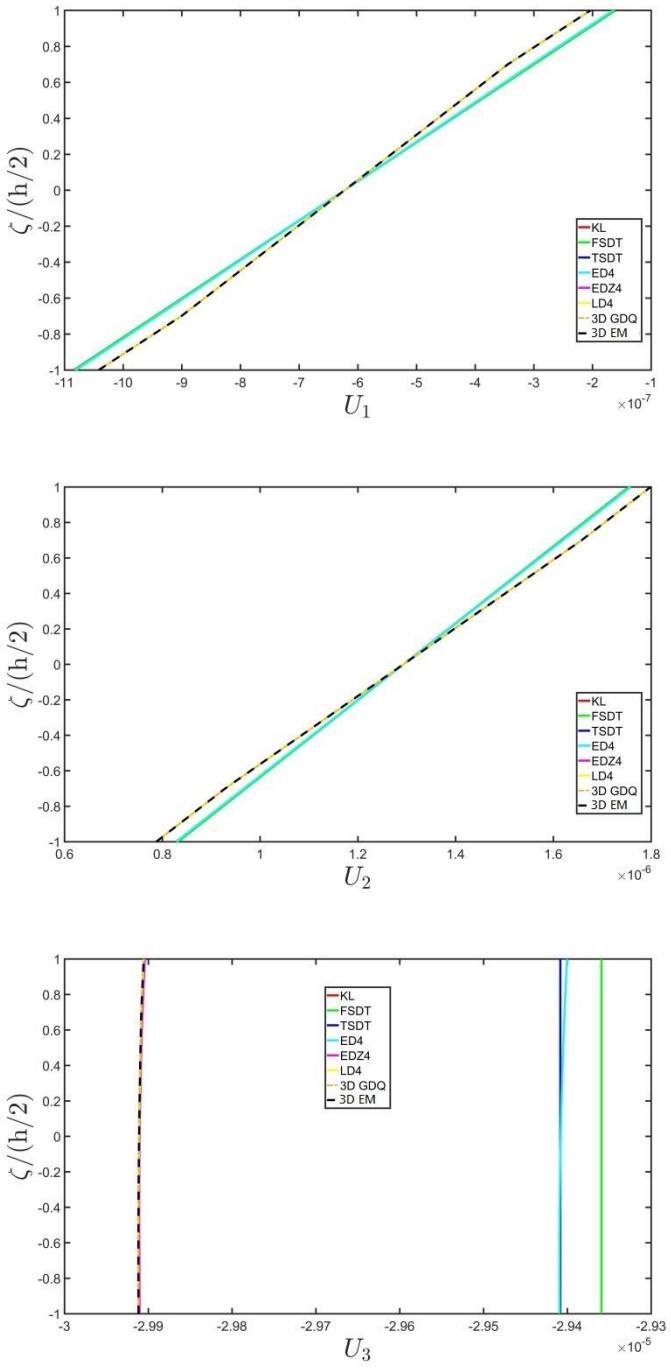

Figure 10. Case 2 $(a/h=100)$: Displacement components [m] along the thickness direction at the point $P=(0.25a,0.25b)$ for a SSSS square sandwich plate made of three layers $(\text{Titanium Alloy / Foam / Titanium Alloy})$ with $h_1=h_3=0.15h$ and $h_2=0.7h$. Transverse shear sinusoidal pressure $q_2^{(+)}=10000\,\text{Pa}$ $(m=1,n=1)$ at the top surface. Comparison between different structural models.

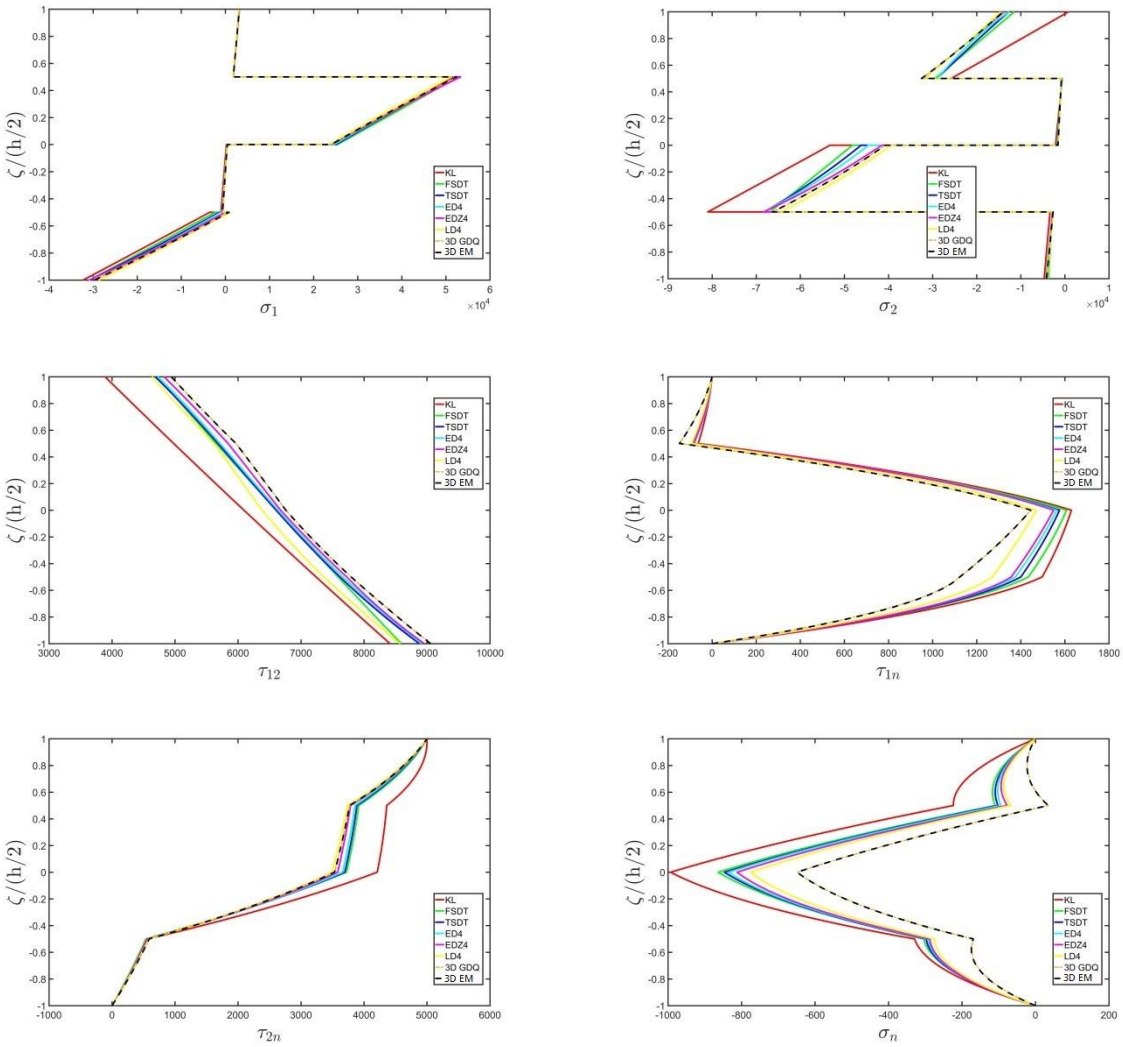

Figure 11. Case 3 $(R/h=20)$: Stress components [Pa] along the thickness direction at the point $P=\left(0.25\left(\alpha_1^1-\alpha_1^0\right),0.25\left(\alpha_2^1-\alpha_2^0\right)\right)$ for a SSSS spherical panel $(R/h=20)$ made of four composite layers $(0/90/0/90)$ with $h_1=h_2=h_3=h_4=h/4$. Transverse shear sinusoidal load $\mathrm{q}_2^{(+)}=10000\,\mathrm{Pa}$ $(m=1,n=1)$ at the top surface. Comparison between different structural models.

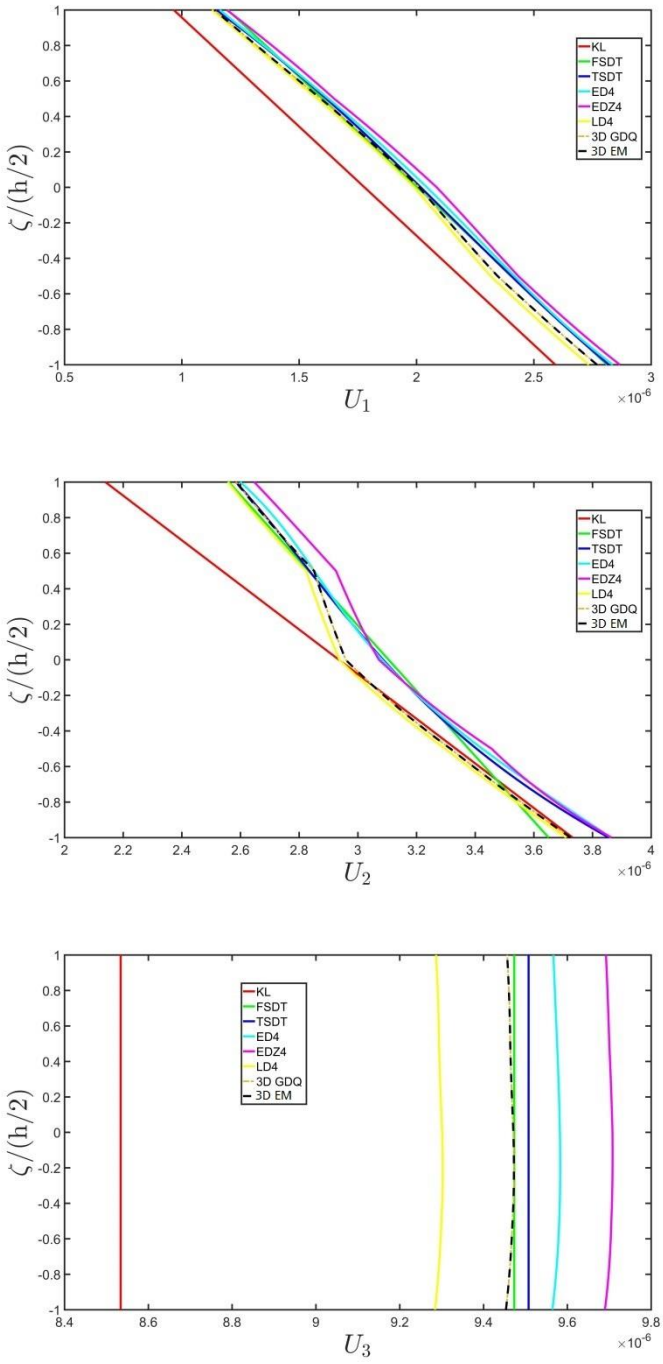

Figure 12. Case 3 $(R/h=20)$: Displacement components [m] along the thickness direction at the point $P=\left(0.25\left(\alpha_1^1-\alpha_1^0\right),0.25\left(\alpha_2^1-\alpha_2^0\right)\right)$ for a SSSS spherical panel $(R/h=20)$ made of four composite layers $(0/90/0/90)$ with $h_1=h_2=h_3=h_4=h/4$. Transverse shear sinusoidal load $\mathrm{q}_2^{(+)}=10000\,\mathrm{Pa}$ $(m=1,n=1)$ at the top surface. Comparison between different structural models.

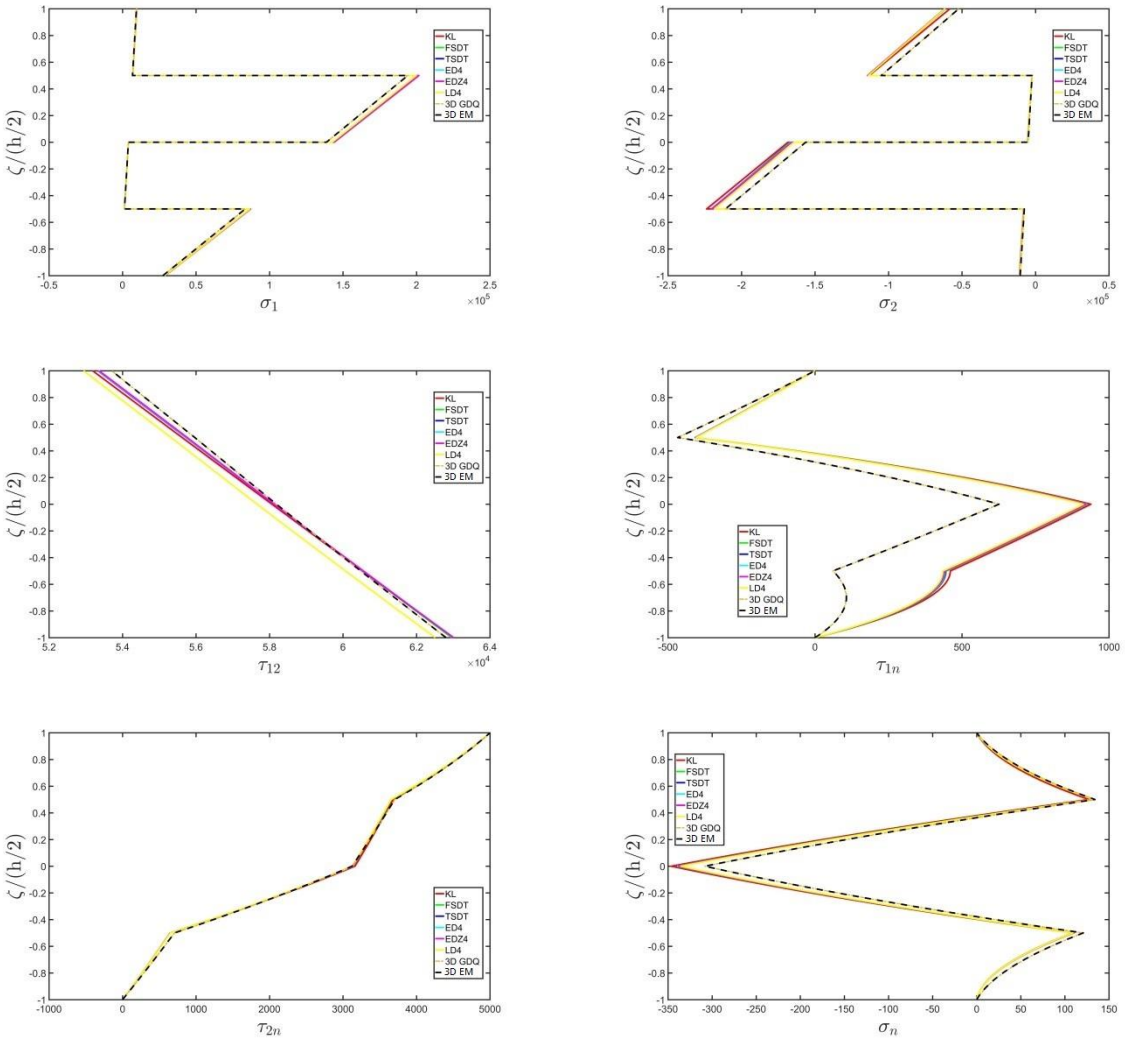

Figure 13. Case 3 $(R/h=100)$: Stress components [Pa] along the thickness direction at the point $P=\left(0.25\left(\alpha_1^1-\alpha_1^0\right),0.25\left(\alpha_2^1-\alpha_2^0\right)\right)$ for a SSSS spherical panel $(R/h=20)$ made of four composite layers $(0/90/0/90)$ with $h_1=h_2=h_3=h_4=h/4$. Transverse shear sinusoidal load $q_2^{(+)}=10000\,\text{Pa}$ $(m=1,n=1)$ at the top surface. Comparison between different structural models.

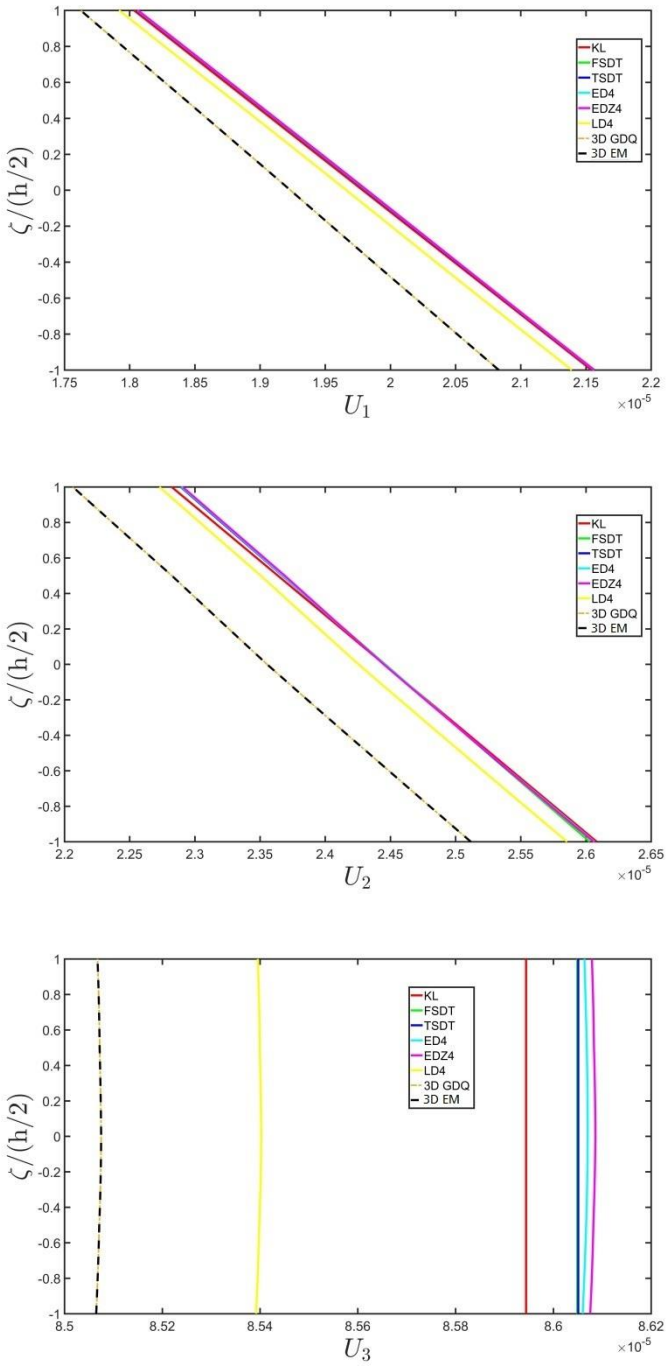

Figure 14. Case 3 $(R/h=100)$: Displacement components [m] along the thickness direction at the point $P=\left(0.25\left(\alpha_1^1-\alpha_1^0\right),0.25\left(\alpha_2^1-\alpha_2^0\right)\right)$ for a SSSS spherical panel $(R/h=20)$ made of four composite layers $(0/90/0/90)$ with $h_1=h_2=h_3=h_4=h/4$. Transverse shear sinusoidal load $q_2^{(+)}=10000\,\text{Pa}$ $(m=1,n=1)$ at the top surface. Comparison between different structural models.

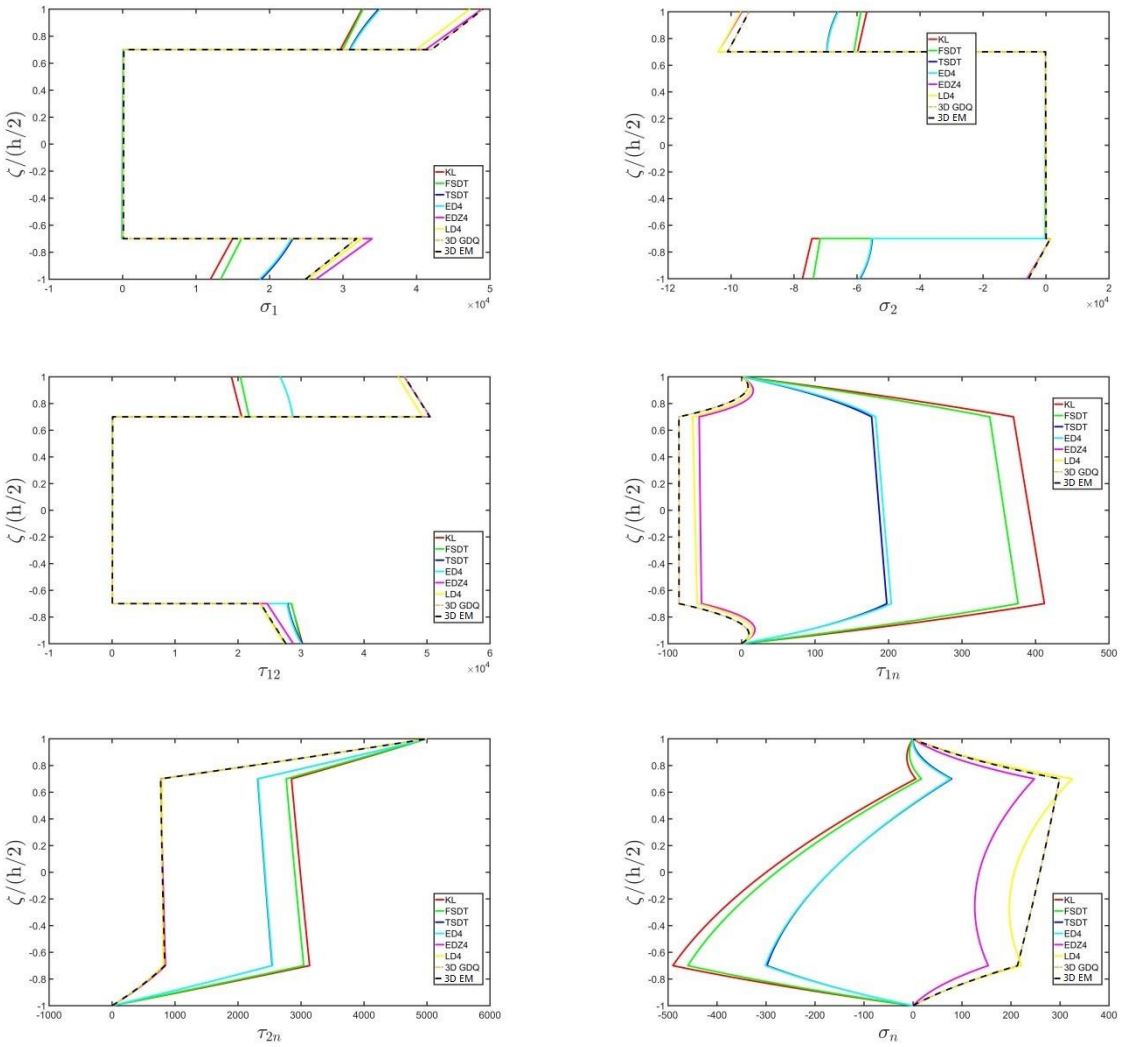

Figure 15. Case 4 $(R/h=20)$: Stress components [Pa] along the thickness direction at the point $P=\left(0.25\left(\alpha_1^1-\alpha_1^0\right),0.25\left(\alpha_2^1-\alpha_2^0\right)\right)$ for a SSSS spherical sandwich panel made of three layers $(\text{Titanium Alloy / Foam / Titanium Alloy})$ with $h_1=h_3=0.15h$ and $h_2=0.7h$ .Transverse shear sinusoidal load $\mathrm{q}_2^{(+)}=10000\,\mathrm{Pa}$ $(m=1,n=1)$ at the top surface. Comparison between different structural models.

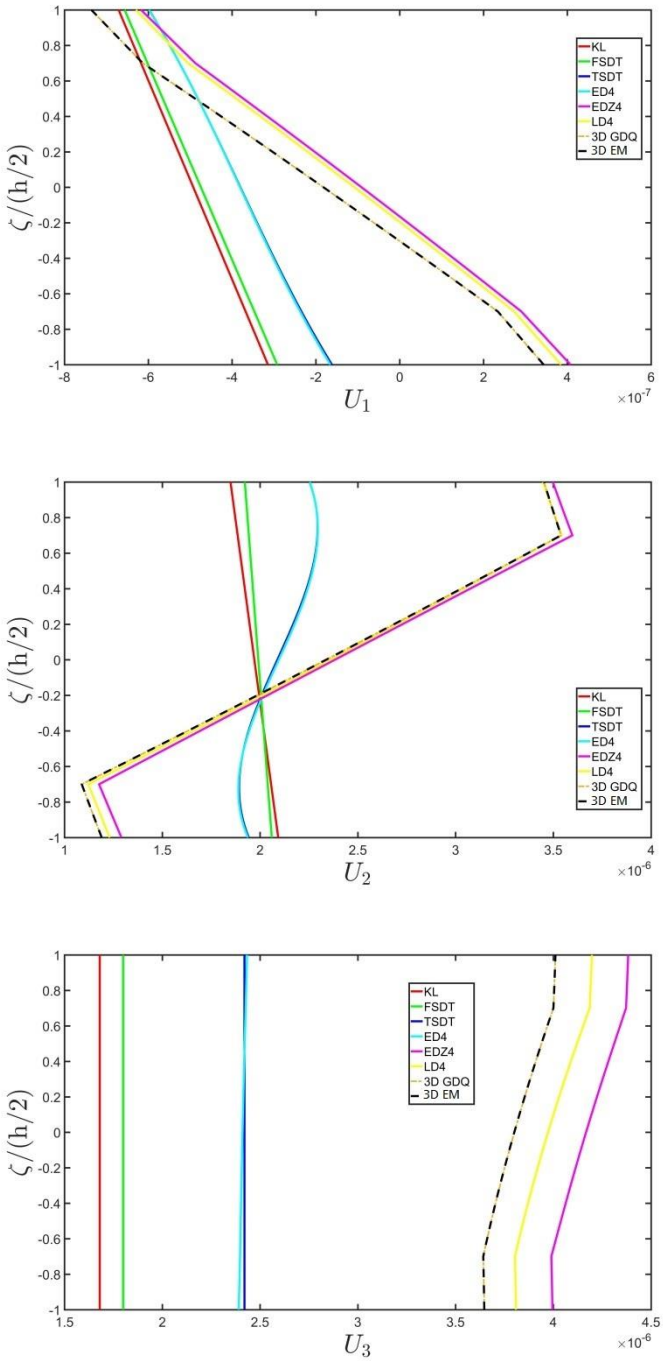

Figure 16. Case 4 $(R/h=20)$: Displacement components [m] along the thickness direction at the point $P=\left(0.25\left(\alpha_1^1-\alpha_1^0\right),0.25\left(\alpha_2^1-\alpha_2^0\right)\right)$ for a SSSS spherical sandwich panel made of three layers $\left(\text{Titanium Alloy / Foam / Titanium Alloy}\right)$ with $h_1=h_3=0.15\,h$ and $h_2=0.7\,h$. Transverse shear sinusoidal load $\mathrm{q}_2^{(+)}=10000\,\mathrm{Pa}$ $(m=1,n=1)$ at the top surface. Comparison between different structural models.

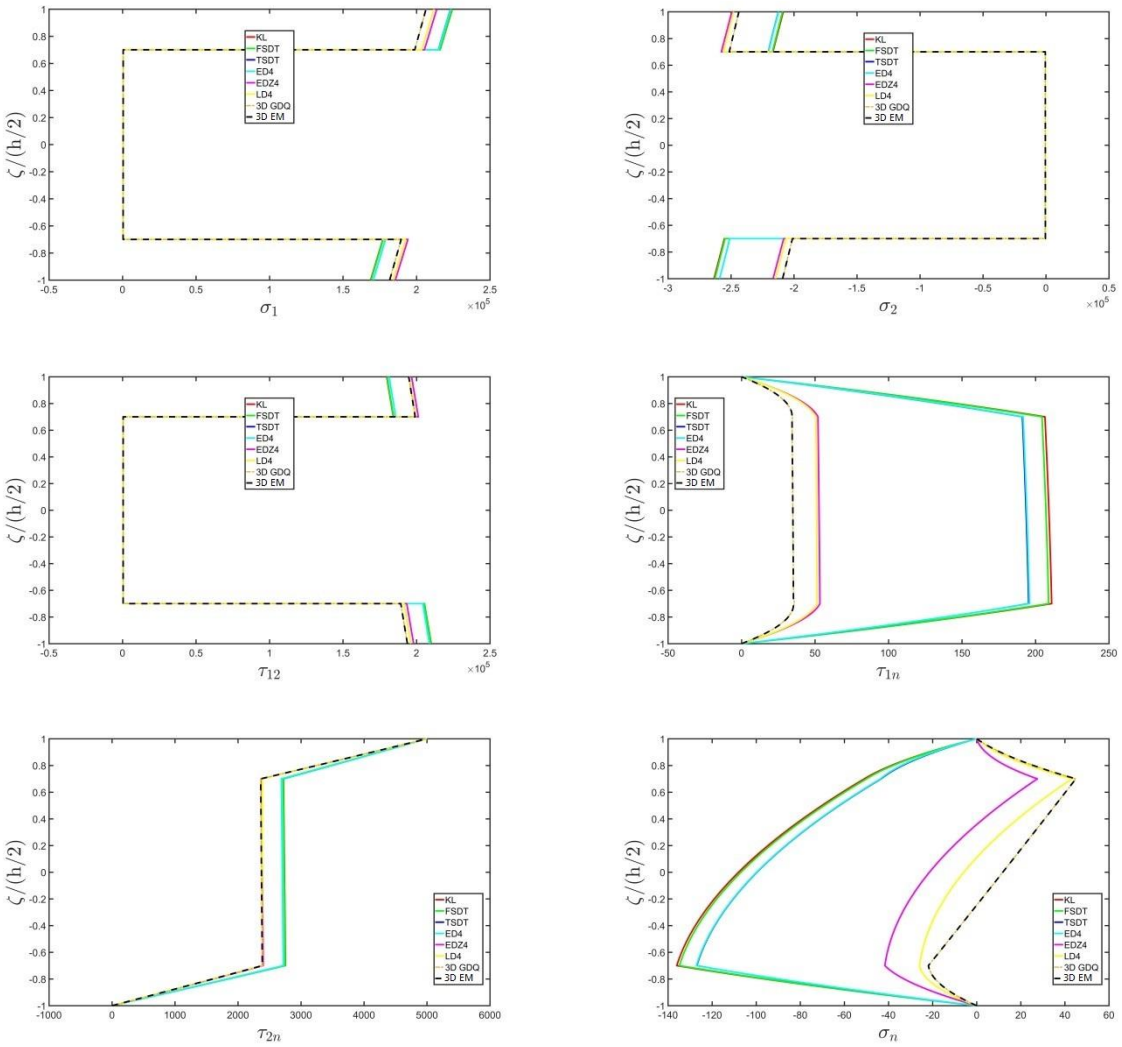

Figure 17. Case 4 $(R/h=100)$: Stress components [Pa] along the thickness direction at the point $P=\left(0.25\left(\alpha_1^1-\alpha_1^0\right),0.25\left(\alpha_2^1-\alpha_2^0\right)\right)$ for a SSSS spherical sandwich panel made of three layers $(\text{Titanium Alloy / Foam / Titanium Alloy})$ with $h_1=h_3=0.15\,h$ and $h_2=0.7\,h$. Transverse shear sinusoidal load $\mathrm{q}_2^{(+)}=10000\,\mathrm{Pa}$ $(m=1,n=1)$ at the top surface. Comparison between different structural models.

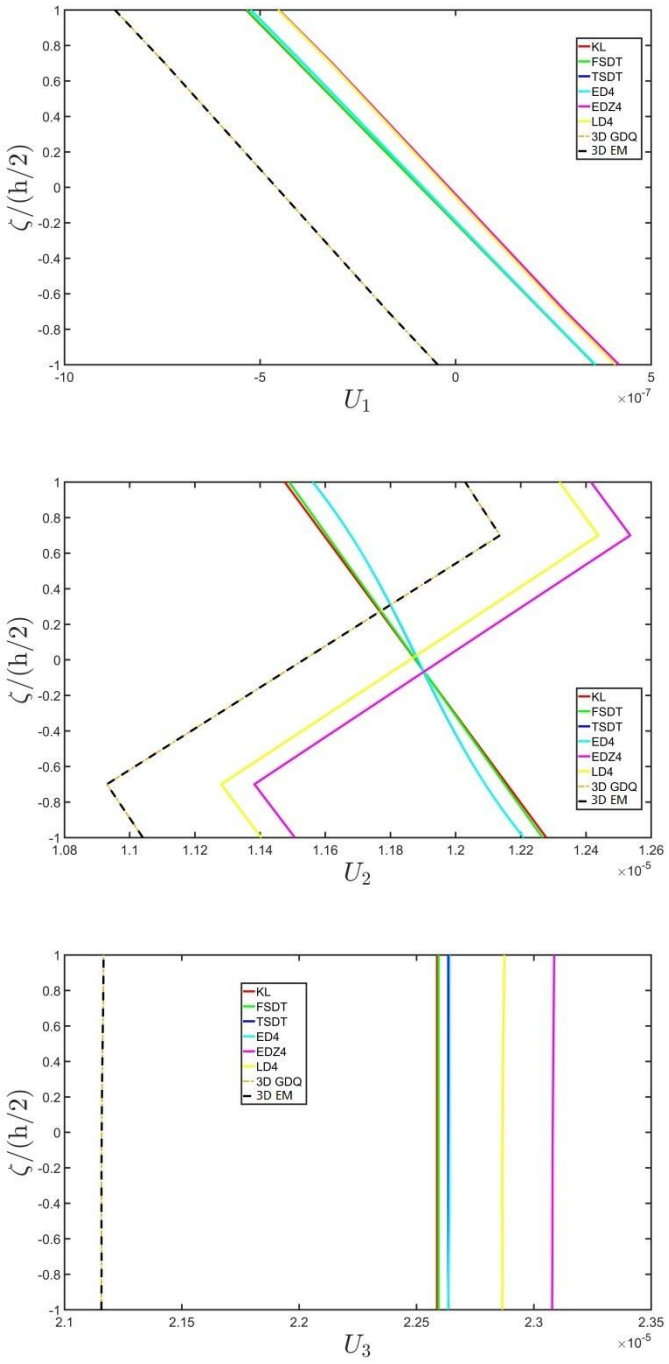

Figure 18. Case 4 $(R/h=100)$: Displacement components [m] along the thickness direction at the point $P=\left(0.25\left(\alpha_1^1-\alpha_1^0\right),0.25\left(\alpha_2^1-\alpha_2^0\right)\right)$ for a SSSS spherical sandwich panel made of three layers $(\text{Titanium Alloy / Foam / Titanium Alloy})$ with $h_1=h_3=0.15\,h$ and $h_2=0.7\,h$ .Transverse shear sinusoidal load $\mathrm{q}_2^{(+)}=10000\,\mathrm{Pa}$ $(m=1,n=1)$ at the top surface. Comparison between different structural models.

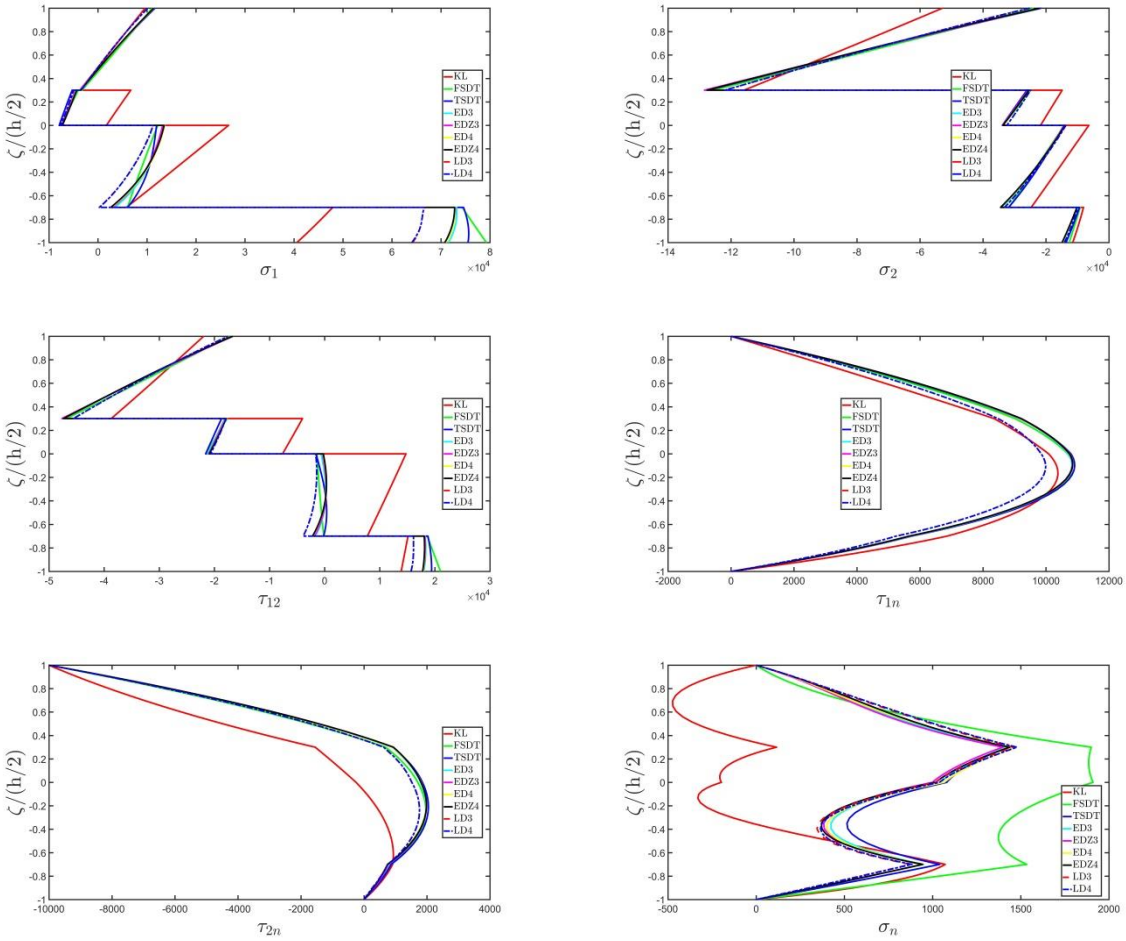

Figure 19. Case 5: Stress components [Pa] along the thickness direction at the point $P=\left(0.75\left(\alpha_1^1-\alpha_1^0\right),0.25\left(\alpha_2^1-\alpha_2^0\right)\right)$ for a CFCF super elliptic panel of revolution made of four composite layers $(20/35/45/70)$ with $h_1=h_4=0.03\,\mathrm{m}$ and $h_2=h_3=0.07\,\mathrm{m}$. Transverse shear uniform load $\mathrm{q}_2^{(+)}=-10000\,\mathrm{Pa}$ at the top surface. Comparison between different structural models.

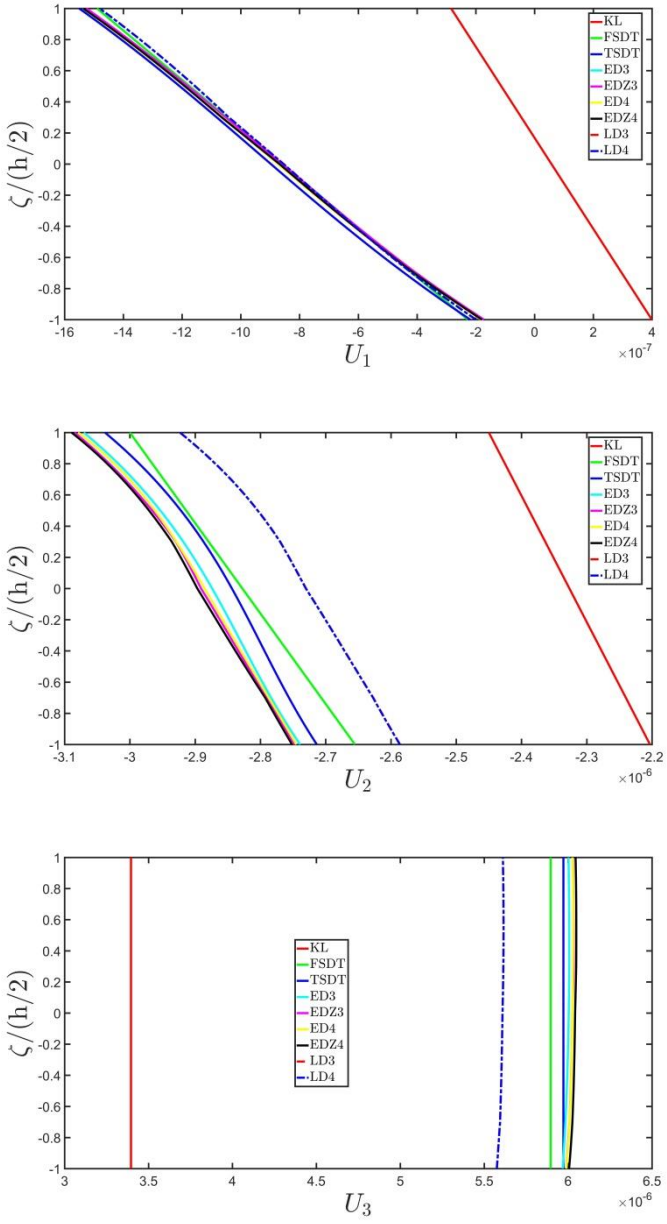

Figure 20. Case 5: Displacement components [m] along the thickness direction at the point $P=\left(0.75\left(\alpha_1^1-\alpha_1^0\right),0.25\left(\alpha_2^1-\alpha_2^0\right)\right)$ for a CFCF super elliptic panel of revolution made of four composite layers $(20/35/45/70)$ with $h_1=h_4=0.03\,\mathrm{m}$ and $h_2=h_3=0.07\,\mathrm{m}$. Transverse shear uniform load $q_2^{(+)}=-10000\,\mathrm{Pa}$ at the top surface. Comparison between different structural models.